Long title: Human demographic history has amplified the effects of background selection across the genome

Short title: Background selection and demography in humans

Raul Torres[1], Zachary A. Szpiech[2], and Ryan D. Hernandez[2,3,4,5*]

[1] Biomedical Sciences Graduate Program, University of California San Francisco, San Francisco, CA, United States of America

[2] Department of Bioengineering and Therapeutic Sciences, University of California San Francisco, San Francisco, CA, United States of America

[3] Institute for Human Genetics, University of California San Francisco, San Francisco, CA, United States of America

[4] Institute for Computational Health Sciences, University of California San Francisco, San Francisco, CA, United States of America

[5] Quantitative Biosciences Institute, University of California San Francisco, San Francisco, CA, United States of America

* Corresponding author

E-mail: ryan.hernandez@ucsf.edu (RDH)

Abstract

Natural populations often grow, shrink, and migrate over time. Demographic processes such as these can impact genome-wide levels of genetic diversity. In addition, genetic variation in functional regions of the genome can be altered by natural selection, which drives adaptive mutations to higher frequencies or purges deleterious ones. Such selective processes impact not only the sites directly under selection but also nearby neutral variation through genetic linkage through processes referred to as genetic hitchhiking in the context of positive selection and background selection (BGS) in the context of purifying selection. While there is extensive literature examining the impact of selection at linked sites at demographic equilibrium, less is known about how non-equilibrium demographic processes impact the effects of hitchhiking and BGS. Utilizing a global sample of human whole-genome sequences from the Thousand Genomes Project and extensive simulations, we investigate how non-equilibrium demographic processes magnify and dampen the consequences of selection at linked sites across the human genome. When binning the genome by inferred strength of BGS, we observe that, compared to Africans, non-African populations have experienced larger proportional decreases in neutral genetic diversity in such regions. We replicate these findings in admixed populations by showing that non-African ancestral components of the genome have also been impacted more severely in these regions. We attribute these differences to the strong, sustained/recurrent population bottlenecks that non-Africans experienced as they migrated out of Africa and throughout the globe. Furthermore, we observe a strong correlation between F_{ST} and inferred strength of BGS, suggesting a stronger rate of genetic drift. Forward simulations of human demographic history with a model of BGS

support these observations. Our results show that non-equilibrium demography significantly alters the consequences selection at linked sites and support the need for more work investigating the dynamic process of multiple evolutionary forces operating in concert.

Author summary

Patterns of genetic diversity within a species are affected at broad and fine scales by population size changes ("demography") and natural selection. From both population genetics theory and observation of genomic sequence data, it is known that demography can alter genome-wide average neutral genetic diversity. Additionally, natural selection can affect neutral genetic diversity regionally across the genome via selection at linked sites. During this process, natural selection acting on adaptive or deleterious variants in the genome will also impact diversity at nearby neutral sites due to genetic linkage. However, less is well known about the dynamic changes to diversity that occur in regions impacted by selection at linked sites when a population undergoes a size change. We characterize these dynamic changes using thousands of human genomes and find that the population size changes experienced by humans have shaped the consequences of linked selection across the genome. In particular, population contractions, such as those experienced by non-Africans, have disproportionately decreased neutral diversity in regions of the genome inferred to be under strong background selection (i.e., selection at linked sites that is caused by natural selection acting on deleterious variants), resulting in large differences between African and non-African populations.

Introduction

Genetic diversity in a species is determined through the complex interplay of mutation, demography, genetic drift, and natural selection. These evolutionary forces operate in concert to shape patterns of diversity at both the local scale and genome-wide scale. For example, in recombining species, levels of genetic diversity are distributed heterogeneously across the genome as peaks and valleys that are often correlated with recombination rate and generated by past or ongoing events of natural selection [1]. But at the genome-wide scale, average levels of genetic diversity are primarily impacted by population size changes, yielding patterns of diversity that are a function of a population's demographic history [2]. These patterns of diversity may also yield information for inferring past events of natural selection and population history, giving valuable insight into how populations have evolved over time [3–8]. With recent advances in sequencing technology yielding whole-genome data from thousands of individuals from species with complex evolutionary histories [9,10], formal inquiry into the interplay of demography and natural selection and testing whether demographic effects act uniformly across the genome as a function of natural selection is now possible.

In the past decade, population genetic studies have shed light on the pervasiveness of dynamic population histories in shaping overall levels of genetic diversity across different biological species. For example, multiple populations have experienced major population bottlenecks and founder events that have resulted in decreased levels of genome-wide diversity. Evidence for population bottlenecks exists in domesticated species such as cattle [11], dogs [12], and rice [13], and in natural populations such as *Drosoph-*

ila melanogaster [14–16], rhesus macaque [17], and humans [18,19]. Notably, population bottlenecks leave long lasting signatures of decreased diversity, which may be depressed even after a population has recovered to or surpassed its ancestral size [20,21]. Such examples are evident in humans, where non-African populations exhibit a lower amount of genetic diversity compared to Africans [9], despite the fact that they have been inferred to have undergone a greater population expansion in recent times [22,23].

Locally (i.e., regionally) across the genome, the action of natural selection can also lead to distinct signatures of decreased genetic diversity (although some forms of selection, such as balancing selection, can increase genetic diversity [24]). For example, mutations with functional effects may be removed from the population due to purifying selection or fix due to positive selection, thereby resulting in the elimination of genetic diversity at the site. But while sites under direct natural selection in the genome represent only a small fraction of all sites genome-wide, the action of natural selection on these selected sites can have far-reaching effects across neutral sites in the genome due to linkage. Under positive selection, genetic hitchhiking [25] causes variants lying on the same haplotype as the selected allele to rise to high frequency during the selection process (note that we will use the term “genetic hitchhiking” here only in the positive selection context of selection at linked sites). Conversely, under purifying selection, background selection (BGS) [26] causes linked neutral variants to decrease in frequency or be removed from the population. Both of these processes of selection at linked sites result in decreased neutral genetic diversity around the selected site. Recombination can decouple neutral sites from selected sites in both cases and neutral diversity

tends to increase toward its neutral expectation as genetic distance from selected sites increases [27].

Evidence for genetic hitchhiking and BGS has been obtained from the genomes of several species, including *Drosophila melanogaster* [28–33], wild and domesticated rice [34,35], nematodes [36,37], humans [3,6,38–42], and others (see [1] for a review). While the relative contributions of genetic hitchhiking and BGS to shaping patterns of human genomic diversity have been actively debated [40,43–45], the data strongly support a large role for BGS in shaping genome-wide patterns of neutral genetic variation [41,42]. Indeed, recent arguments have been made in favor of BGS being treated as the null model when investigating the impact of selection at linked sites across recombining genomes [1,32,45–48], with one study in humans showing that BGS has decreased genetic diversity by 19-26% if other modes of selection at linked sites are assumed to be minor [6].

Although the effects of selection at linked sites across the genome have been described in a multitude of studies, it is still less obvious whether populations that have experienced different demographic histories, such as African and non-African human populations, should exhibit similar relative effects in those regions. In the context of BGS, early work resulted in the expression $\pi \approx 4f_0N_e\mu$ [26], which suggests that the expected level of diversity with BGS is simply proportional to the neutral expectation (with proportionality constant f_0 being a function of the rates of deleterious mutation and recombination). Importantly, while populations with different N_e are expected to have different levels of π in the context of BGS, the proportionality constant f_0 is assumed to be independent of population history (so long as the recombination landscape and delete-

rious mutation rates remain constant). Much of the theory developed in the context of BGS has been developed under the assumption that the population is at demographic equilibrium, and recent work has demonstrated that this assumption likely holds under changing demography if selection is strong enough (or populations are large enough) such that mutation-selection balance is maintained [49,50]. However, strong, sustained population bottlenecks may lead to violations of that assumption. Thus, in humans and other natural populations experiencing non-equilibrium demography, genetic drift may perturb genetic diversity at neutral sites under BGS that are unaccounted for in these models.

While little attention has been given to the potential consequences of demography on patterns of neutral variation in regions experiencing selection at linked sites (but see [51,52] for how selection at linked sites may impact the inference of demography itself), recent studies have suggested that alleles directly under natural selection experience non-linear dynamics in the context of non-equilibrium demography. For the case of purifying selection, the equilibrium frequency of an allele is dependent on its fitness effect, with deleterious alleles having lower equilibrium frequencies than neutral alleles. After a population size change, deleterious alleles tend to change frequency faster than neutral alleles, allowing them to reach their new equilibrium frequency at a faster rate [53,54]. This can result in relative differences in deleterious allele frequencies among populations with different demographic histories. Such effects are especially apparent in populations suffering bottlenecks [55] and have been tested and observed between different human populations with founder populations exhibiting a greater proportion of non-synonymous variation relative to synonymous variation [56–58]. We hypothesized

139 that these non-equilibrium dynamics could also perturb nearby neutral variants due to
140 the effects of selection at linked sites. In support of our hypothesis, a recent simulation
141 study modeling *Drosophila* observed that population bottlenecks can result in different
142 rates of recovery of neutral genetic diversity depending on the strength of BGS [48].
143 Another recent study [59] analyzed neutral diversity surrounding putatively deleterious
144 loci in domesticated versus wild maize. They found that the extreme domestication bot-
145 tleneck reduced the efficiency of purifying selection, which has resulted in higher rela-
146 tive diversity in the domesticated population compared to the wild population (which has
147 likely experienced a much more stable demographic history). Together, these studies
148 provide further evidence that non-equilibrium demography should have a strong effect
149 on patterns of diversity in the presence of selection at linked sites.

150 To investigate the impact of non-equilibrium dynamics in regions experiencing
151 selection at linked sites, we measure patterns of average pairwise neutral genetic diver-
152 sity (π), or neutral heterozygosity if the population was admixed, as a function of the
153 strength of BGS, *B* (inferred by Ref. [6]), within a global set of human populations from
154 phase 3 of the Thousand Genomes Project (TGP) [9]. We focus on the ratio of neutral
155 diversity in regions of strong BGS (low *B*) to regions of weak BGS (high *B*, the closest
156 proxy available for neutral variation in humans), which we term "relative diversity." While
157 there are many caveats that may plague the direct interpretation of specific *B* values
158 (e.g., positive selection is not modeled, the distribution of fitness effects are inconsistent
159 with other studies, and the deleterious mutation rate exceeds the per base pair mutation
160 rate of other studies), we argue below that *B* scores nevertheless provide a decent

proxy for ranking sites from most closely linked to deleterious loci (low *B*) to most unlinked from deleterious loci (high *B*) in humans.

We find substantial differences in relative diversity between populations, which we attribute to their non-equilibrium demographics. We confirm that the interplay of demography and selection at linked sites can explain the differences of relative diversity across human populations with simulations incorporating a parametric demographic model of human history [7] with and without a model of BGS. We also investigate how genetic differentiation between TGP populations (as measured by F_{ST}) is shaped by selection at linked sites by measuring F_{ST} as a function of *B*. Finally, we demonstrate that back migration from Europeans and Asians into Africa re-introduces sufficient deleterious variation to impact patterns of BGS, leading to decreased relative diversity in Africans. Our results demonstrate the strong impact that changing demography has on perturbing levels of diversity in regions experiencing selection at linked sites and have implications for population genetic studies seeking to characterize linked selection across any species or population that is not at demographic equilibrium.

Results

Differential impact of selection at linked sites across human populations

We measured mean pairwise genetic diversity (π) in the autosomes (we ignore the sex chromosomes and the mitochondrial genome for all analyses) among the 20 non-admixed populations from the phase 3 TGP data set, consisting of 5 populations each from 4 continental groups: Africa (AFR), Europe (EUR), South Asia (SASN), and East Asia (EASN; population labels and groupings reported in S12 Table in Supporting

184 information). A set of stringent filters, including the masking of sites inferred to be under
185 selective sweeps, were first applied to all 20 populations to identify a high-quality set of
186 putatively neutral sites in the genome (see Materials and Methods). Sites were then di-
187 vided into quantile bins based on *B* [6]. For our initial set of analyses, we focused on the
188 bins corresponding to the 1% of sites inferred to be under the strongest amount of BGS
189 (i.e., sites having the lowest inferred *B* values) and the 1% of sites inferred to be under
190 the weakest amount BGS (i.e., sites having the highest inferred *B* values). Mean diversi-
191 ty was normalized by divergence with rhesus macaque within these bins for each popu-
192 lation and is shown in Figs 1A-B. As expected, normalized diversity was highest in Afri-
193 can populations and lowest in East Asian populations across both 1% *B* quantile bins.

194 To estimate the impact that selection at linked sites has had on neutral diversity,
195 we calculated a statistic called "relative diversity" (analogous to π/π_0 in the BGS litera-
196 ture; [26,60]) for each population. We define relative diversity as the ratio of normalized
197 diversity in the lowest 1% *B* bin to normalized diversity in the highest 1% *B* bin, which
198 should capture the relative impact of selection at linked sites within the genome. Fig 1C
199 shows that relative diversity was lower in non-African populations (0.348-0.365 for non-
200 Africans, 0.396-0.408 for Africans), suggesting that these populations have experienced
201 a greater reduction in diversity due to selection at linked sites than can be explained by
202 demography alone.

203 To characterize these effects across a broader distribution of sites experiencing
204 selection at linked sites, we grouped populations together according to their continental
205 group (i.e., African, European, South Asian, and East Asian, see S12 Table in Support-
206 ing information for a detailed description) and estimated relative diversity at neutral sites

for each of the continental groups in bins corresponding to the lowest 1%, 5%, 10%, and 25% quantiles of *B* (note these partitions were not disjoint). As expected, relative diversity increased for all continental groups as the bins became more inclusive (Fig 2B), reflecting a reduced impact on the reduction of diversity due to selection at linked sites. We also observed that non-African continental groups consistently had a lower relative diversity compared to African groups, demonstrating that the patterns we observed in the most extreme regions experiencing selection at linked sites also held for broader regions. Interestingly, we observed a consistent trend of rank order for relative diversity between the different continental groups for each quantile bin, with the East Asian group experiencing the greatest reduction of relative diversity, followed by the South Asian, European, and African groups. This result suggested a stronger effect for demography on the diversity-reducing effect selection at linked sites for those populations experiencing the strongest bottlenecks. However, the observed differences in relative diversity between non-African and African continental groups became less pronounced as the bins became more inclusive (Fig 2B). These effects remained even after we controlled for the effects of GC-biased gene conversion and recombination hotspots (S2 and S4 Figs) or if we did not normalize diversity by divergence (S3 and S5 Figs). Patterns of relative diversity in regions of local ancestry (i.e., African, European, or Native American) across admixed TGP populations also largely recapitulated the patterns observed in their continental group counterparts across *B* quantile bins, with the largest reductions in relative diversity occurring for the Native American and European ancestral segments (S11 Fig, S1 Supporting information).

229 To test if demography has impacted selection at linked sites more recently in
230 time, we also calculated the number of singletons observed per site (normalizing by di-
231 vergence and using the same set of neutral filters as was used for the calculations of π)
232 across the lowest and highest 1% *B* quantile bins. Singletons are, on average, the
233 youngest variants within the genome and should better capture signals about more re-
234 cent population history. We took the ratio of singletons observed per-site across these
235 extreme *B* quantile bins to create a statistic called relative singleton density, which we
236 term "ψ/ψ_0." We accounted for differences in population sample size by first projecting
237 down all populations to 2N=170 (Materials and methods). Qualitatively, our measure-
238 ments of ψ/ψ_0 showed patterns in the opposite direction of our calculations of π/π_0, with
239 Africans exhibiting a lower ratio of ψ/ψ_0 when compared to non-Africans (0.665-0.695
240 for Africans, 0.733-0.804 for non-Africans; Fig 3). These patterns suggest that the im-
241 pact of demography on regions experiencing selection at linked sites is transient, with
242 patterns of relative diversity between populations dependent on the time frame in which
243 they are captured (see Discussion).
244

245 **Selection at linked sites has shaped patterns of population differentiation**

246 We have shown that selection at linked sites increases the rate of drift at neutral
247 loci, and that this process is amplified by demographic changes like population bottle-
248 necks. One might then expect that selection could also amplify population differentiation
249 at linked neutral loci. This outcome is obvious in the context of hitchhiking (where linked
250 neutral loci sweep to high frequency) but is also expected with BGS [61,62], since de-
251 creases in diversity can accelerate differentiation. Here we quantify the magnitude of

the effect of BGS on population differentiation in humans, and find that population differentiation at neutral loci is indeed highly correlated with *B* (the inferred strength of BGS; Fig 4 and Table 1). Specifically, we divided the genome into 2% quantile bins based on the genome-wide distribution of *B* and measured F_{ST} in each bin for all pairs of populations from different continental groups [63]. We then performed simple linear regression using *B* as an explanatory variable and F_{ST} as our dependent variable with the linear model $F_{ST} = \beta_0 + \beta_1 B + \varepsilon$. We found that across all 150 population comparisons (i.e., the "Global" estimate in Table 1), *B* explained 26.9% of the change in F_{ST} across the most extreme *B* values, was robust to outliers [64] (S6 Table in Supporting information), and dominated the effects of local recombination rate (see Supporting information).

Table 1. Regression coefficient estimates for linear regression of F_{ST} on 2% quantile bins of *B*.

	AFR vs. EASN	AFR vs. EUR	AFR vs. SASN	EUR vs. SASN	EUR vs. EASN	SASN vs. EASN	Global
β_0 ± SEM (*p*)	0.2044 ± 0.0039 (< 1e-04)	0.1716 ± 0.0031 (< 1e-04)	0.1596 ± 0.0029 (< 1e-04)	0.0455 ± 0.0011 (< 1e-04)	0.1216 ± 0.0029 (< 1e-04)	0.0903 ± 0.0023 (< 1e-04)	0.1322 ± 0.0019 (< 1e-04)
β_1 ± SEM (*p*)	-0.0434 ± 0.0046 (< 1e-04)	-0.0358 ± 0.0037 (< 1e-04)	-0.0355 ± 0.0034 (< 1e-04)	-0.0098 ± 0.0013 (< 1e-04)	-0.0173 ± 0.0035 (< 1e-04)	-0.0261 ± 0.0027 (< 1e-04)	-0.0280 ± 0.0022 (< 1e-04)
r ± SEM	-0.8363 ± 0.0295	-0.7441 ± 0.0362	-0.7794 ± 0.0332	-0.3847 ± 0.0414	-0.6220 ± 0.0785	-0.5968 ± 0.0348	-0.1292 ± 0.0098

The first two rows give the regression coefficients for the linear model $F_{ST} = \beta_0 + \beta_1 B + \varepsilon$, where *B* represents the mean background selection coefficient for the bin being tested and F_{ST} is the estimated F_{ST} for all population comparisons within a particular pair of continental groups (given in the column header). The final column, "Global", gives the regression coefficients for the linear model applied to all pairwise population comparisons (150 total). The correlation coefficient, *r*, between *B* and F_{ST} for each comparison is shown in the bottom row. Standard errors of the mean (SEM) for β_0, β_1, and *r* were calculated from 1,000 bootstrap iterations (see Materials and Methods). P-values are derived from a two-sided t-test of the t-value for the corresponding regression coefficient.

277

278 **Demographic inference in putatively neutral regions of the genome**

279 One consequence of BGS and hitchhiking in driving patterns of neutral variation
280 within and between human populations is that demographic inference could be substan-
281 tially biased [51,52,65]. To assess the degree of bias in the context of human data, we
282 fit a 13-parameter demographic model of African, European, and East Asian demogra-
283 phy using only putatively neutral regions of the genome under the weakest effects of
284 selection at linked sites ($B \geq 0.994$) from a subset of TGP individuals with high coverage
285 whole genome sequence data (see Materials and Methods). Our demographic model
286 followed that of Gutenkunst et al. [7], with an ancient human expansion in Africa and a
287 single out-of-Africa bottleneck followed by European- and East Asian-specific bottle-
288 necks, as well as exponential growth in both non-African populations and migration be-
289 tween all populations. To make comparisons to previous studies that have used se-
290 quence data from coding regions or genes [7,22,23], which may be under strong BGS
291 or hitchhiking effects, we also inferred demographic parameters using coding four-fold
292 degenerate synonymous sites. Our inferred parameters for human demography were
293 strikingly different between the two sets of sequence data (S1 Fig, S1 Table in Support-
294 ing information). Notably, inferred effective population size parameters were larger for
295 contemporary population sizes when using four-fold degenerate synonymous sites ver-
296 sus ascertained neutral regions with $B \geq 0.994$, with N_e inferred to be 22%, 23%, and
297 29% larger for AFR, EUR, and EASN populations, respectively. This is despite the fact
298 that the ancestral N_e was inferred to be lower for four-fold degenerate synonymous sites
299 (N_e = 18,449 and 17,118, for neutral regions with $B \geq 0.994$ and four-fold degenerate

300 sites, respectively). This result may stem from the expected decrease in N_e going into
301 the past in regions of strong BGS, which can lead to inflated estimates of recent popula-
302 tion growth [52] and has also been shown in simulation studies of synonymous sites
303 under BGS [65]. Put more simply, the skew of the site-frequency spectrum towards rare
304 variants in regions experiencing selection at linked sites mimics a population expansion,
305 thus leading to erroneous inference.
306

307 **Simulations confirm that demographic effects can impact background selection**

308 Using the demographic parameters inferred from neutral regions where $B \geq$
309 0.994, we simulated patterns of neutral diversity with and without the effects BGS (see
310 Materials and Methods). To measure the relative impact of BGS for each population, we
311 then took the ratio of neutral diversity from BGS simulations (π) and neutral diversity
312 from simulations without BGS (π_0) to calculate relative diversity (π/π_0). As expected, we
313 found that BGS reduced relative diversity ($\pi/\pi_0 < 1$) for all three populations in our simu-
314 lations. However, non-African populations experienced a proportionally larger decrease
315 in π/π_0 compared to the African population (π/π_0 = 0.43, 0.42, 0.41 in AFR, EUR, and
316 EASN respectively). These results are comparable to (but not quite as extreme as) the
317 effects we observed in the regions of the genome with the strongest effects of BGS for
318 these population groups (Fig 1C). To understand how this dynamic process occurs, we
319 sampled all simulated populations every 100 generations through time to observe the
320 effect of population size change on π, π_0, and the ratio π/π_0 (Fig 5). We observed that
321 there is a distinct drop in π and π_0 at each population bottleneck experienced by non-
322 Africans, with East Asians (who had a more severe bottleneck) experiencing a larger

drop than Europeans. Fig 5C shows that the population bottlenecks experienced by non-African populations also reduces π/π_0. Surprisingly, Africans also experienced a large drop in π/π_0 (but less than non-Africans) even though they did not experience any bottlenecks. This was attributable to migration between non-Africans and Africans and this pattern disappeared when we ran simulations using an identical demographic model with BGS but without migration between populations (S7 Fig). This finding highlights an evolutionary role that deleterious alleles can play when they are transferred across populations through migration (see Discussion).

We also calculated ψ/ψ_0 across these simulations and again qualitatively observed patterns similar to, but not as extreme, as our empirical calculations of ψ/ψ_0. As with pairwise neutral diversity, BGS predictably decreased the density of singletons across all populations (S12 Fig A). However, Africans exhibited a lower ψ/ψ_0 when compared to non-Africans (ψ/ψ_0 = 0.79, 0.89, 0.91 in AFR, EUR, and EASN respectively). Calculating ψ and ψ_0 through time showed that the population bottlenecks experienced by non-Africans led to strong decreases in both ψ and ψ_0, with recent expansion in these populations then leading to large, rapid recoveries. Strong decreases in ψ/ψ_0 after each population bottleneck were also observed, including a slight decrease in ψ/ψ_0 in Africans that disappeared in the simulations without migration (S12 Fig B). While ψ/ψ_0 for the European/East Asian ancestral population in the simulations with migration remained below that of Africans during the course of the Out-of-Africa bottleneck, we observed a rapid recovery in ψ/ψ_0 for this population in the simulations without migration (compare bottoms panels, S12 Fig A and B). This suggests that for populations experiencing a sustained population bottleneck, the response of singletons to changes in the

346 weakened intensity of BGS is quite rapid, especially when compared to patterns of π/π_0
347 (compare Fig S7 C to Fig S12 B bottom panel). However, population migration mitigates
348 this pattern. However, regardless of whether migration between populations was simu-
349 lated, BGS seemed to have little effect on singleton density recovery in Europeans and
350 Asians once population expansion occurred.

351 Our simulations were based on the functional density found in a 2 Mb region of
352 the human genome with the lowest *B* values and, thus, where BGS was inferred to be
353 strongest (chr3: 48,600,000-50,600,000). There, 20.46% of sites were either coding or
354 conserved non-coding (see Materials and Methods). Thus, the fraction of the genome
355 experiencing deleterious mutation in our simulations of strong BGS was 0.2046. The
356 patterns we observed in these simulations likely represent an upper bound on the
357 strength of BGS in the human genome. Since the strength of BGS is dependent upon
358 the density of sites experiencing deleterious mutation within a given region (or more
359 formally, *U*, which is the product of the per-site deleterious mutation rate and the num-
360 ber of sites experiencing deleterious mutation [66]), we simulated weaker effects of
361 BGS by reducing the fraction of sites experiencing purifying selection (keeping the dis-
362 tribution of selective effects constant, see Materials and Methods). When the fraction of
363 sites experiencing selection was decreased 2-4 fold in our simulations, we continued to
364 observe a stepwise decrease in π/π_0 while maintaining the specific rank order of African,
365 followed by European, and then East Asian populations (S8 Fig). As expected, π/π_0 in-
366 creased for all populations as the fraction of sites that were simulated as deleterious
367 decreased (π/π_0 = 0.641 vs. 0.802, 0.62 vs. 0.777, and 0.611 vs. 0.777 for AFR, EUR,
368 and EASN when the fraction of sites experiencing selection was reduced to 0.1023 and

369 0.05115, respectively). These simulations resulted in π/π_0 values much larger than we
370 observed in data (Figs 1C, 2B).
371

372 ## Discussion

373 In our analyses of thousands of genomes from globally distributed human popu-
374 lations, we have confirmed that the processes of demography and selection at linked
375 sites govern neutral variation across the genome. While this observation is not unex-
376 pected, we have characterized the dynamic consequence of non-equilibrium demo-
377 graphic processes in regions experiencing selection at linked sites in humans. We find
378 that demography (particularly population bottlenecks) can amplify the consequences of
379 selection at linked sites. To remove any possible biases that would influence our results,
380 we controlled for functional effects of mutations, variability in mutation along the ge-
381 nome, potential sequencing artifacts, GC-based gene conversion, the potential muta-
382 genic effects of recombination hotspots, and also removed regions of the genome with
383 signatures of positive selection. None of these factors qualitatively affected our results.
384 We do recognize that one caveat of our controls is the fact that divergence itself
385 is not independent of BGS [67], and this may present biases when using divergence to
386 control for variation in mutation rate along the genome. This is because the rate of coa-
387 lescence in the ancestral population of two groups will be faster in regions of strong
388 BGS compared to regions of weak BGS due to the lower N_e of the former, leading to a
389 decrease in overall divergence in those regions. To limit the contribution of such biases
390 in ancestral N_e to divergence, we use rhesus macaque since it is more distantly related
391 to humans than other primate species such as orangutan or chimpanzee (human-

392 rhesus divergence: 29.6 MYA; [68]). Furthermore, if *B* truly captures the effects of BGS,
393 then normalizing by the lower divergence that is characteristic of strong BGS bins and
394 the higher divergence that is characteristic of weak BGS bins should make any differ-
395 ences between the two smaller, not greater. In fact, for our calculations of relative diver-
396 sity in which we skip the normalization step, the differences in diversity between the
397 lowest 1% and highest 1% *B* value bins are greater and give a lower ratio of relative di-
398 versity (π/π_0 for AFR is 0.373 without the divergence step and 0.402 with the divergence
399 step). A similar pattern is also observed for other continental groups (compare Fig 2 and
400 S5 Fig). More importantly though, we should not expect the potential biases of our di-
401 vergence step to contribute to the differences in relative diversity between each of the
402 continental groups since biases in divergence estimates across the genome are based
403 on the human reference sequence and are therefore identical across all human popula-
404 tions.

405 We also note that the estimates of *B* by McVicker et al. [6] may be biased by
406 model assumptions concerning mutation rates and the specific sites subject to purifying
407 selection, with the exact values of *B* unlikely to be precisely inferred. In fact, the *B* val-
408 ues provided by McVicker et al. range from 0 to 1, suggesting that some regions of the
409 genome should be essentially devoid of diversity (but we do not observe this to be the
410 case). Since our own analyses show that relative diversity has a lower bound at only
411 ~0.35 in humans, the exact value of *B* itself should not be taken at face value. Rather,
412 our primary motivation for using *B* was to ascertain regions that should be on the ex-
413 treme ends of the genome-wide distribution of regions experiencing selection at linked
414 sites, for which *B* should provide a good assessment. A study by Comeron et al. [32]

415 that investigated BGS in *Drosophila* and utilized the same model of BGS as McVicker et
416 al. found that biases presented by model assumptions or mis-inference on the exact
417 value of *B* do not significantly change the overall rank order for the inferred strength of
418 BGS across the genome. Thus we, expect McVicker et al.'s inference of *B* to provide
419 good separation between the regions experiencing the weakest and strongest effects of
420 selection at linked sites within the human genome, with model misspecification unlikely
421 to change our empirical results.

422 While the effects of selection at linked sites in humans captured in our analyses
423 could in principle include the consequences of positive selection, such as soft-sweeps
424 and classic selective sweeps, we applied stringent filters to remove any such regions
425 before our analysis (Materials and methods, S1 Appendix). We therefore expect that
426 most of the resulting patterns we observe can be attributed to the consequences of
427 BGS. Recently, a joint model of classic selective sweeps and BGS was applied to *Dro-*
428 *sophila* and predicted that BGS has had a ~1.6 to 2.5-fold greater effect on neutral ge-
429 netic diversity than classic selective sweeps [33], with another study giving similar re-
430 sults [69]. We should expect this magnitude to be even greater for humans, since clas-
431 sic selective sweeps were found to be rare in recent human evolution [41] and adaptive
432 substitutions in the human genome are much less frequent than in *Drosophila* [5,70,71].
433 Nonetheless, we cannot rule out all contributions from hitchhiking to our results. In fact,
434 our own simulations of BGS fail to capture the complete effects of linked selection on
435 reducing π/π_0 in different human populations (compare Figs 1C and 5C) and the addi-
436 tional contribution of hitchhiking to humans, which we did not simulate, may explain this
437 discrepancy.

438 Non-equilibrium demography has also been of recent interest in regards to its
439 impact on patterns of deleterious variation across human populations (often referred to
440 as genetic load), with initial work showing that non-African populations have a greater
441 proportion of non-synonymous deleterious variants that are homozygous compared to
442 synonymous variants [56]. Similar results in human founder populations [57,72],
443 *Arabadopsis* [73], and domesticated species such as dogs [12] and sunflowers [74]
444 further demonstrate the pervasive impact that demography has on influencing the
445 relative amount of deleterious variation across a variety of populations and species.
446 Since BGS is a function of deleterious variation, it is not surprising that we also witness
447 differences in π/π_0 across human populations that have experienced different
448 demographic histories. These effects are likley ubiquitous across other species as well.
449 However, there has been recent contention about whether the previously described
450 patterns of increased deleterious variation are driven by a decrease in the efficacy of
451 natural selection (thus resulting in increased genetic load) or are solely artifacts of the
452 response of deleterious variation to demographic change [58,75–78]. Recently, Koch et
453 al. [55] investigated the temporal dynamics of demography on selected sites within
454 humans and observed that after a population contraction, heterozygosity at selected
455 sites can undershoot its expected value at equilibrium as low-frequency variants are lost
456 at a quicker rate before the recovery of intermediate frequency variants can occur. In
457 the context of both BGS and hitchhiking, which skew the site frequency spectrum of
458 linked neutral mutations towards rare variants [26,66,79,80], we also expect a transient
459 decrease in diversity as low-frequency variants are lost quickly during a population
460 contraction. Indeed, as evident from our simulations of BGS and demography,

immediatley after a population bottleneck, rapid losses in singleton density can occur, leading to transient decreases in ψ/ψ_0. However, the recovery in singleton density is also quite rapid, while the recovery in π and π/π_0 is quite slow. This is due to the fact that higher frequency variants, which contribute a greater amount to π, take a longer amount of time to recover after a population contraction compared to lower-frequency variants such as singletons. However, Koch et al. also demonstrated that the effect of demography on diversity is only temporary and that long-term diversity at selected sites approaches greater values once equilibrium is reached. We also stress these temporal effects on the patterns of relative neutral diversity that we observe here. In the context of BGS, if no population recovery occurs following a contracation, deleterious variants may behave more neutrally, weaking the overall effect of BGS and causing π/π_0 to become larger than in the ancestral, pre-bottleneck population.

The temporal effects of non-equilbrium demographics on patterns of π/π_0 and ψ/ψ_0 may also explain the conflicting results obtained in a similar study of selection at linked sites in teosinte and its domesticated counterpart, maize [59]. In that study, the authors observed that π/π_0 was higher in maize, which underwent a population bottleneck during domestication (no bottleneck event was inferred for the teosinte population) but that ψ/ψ_0 was also lower. This result is contrary to what we observed qualitatively between non-African and African human populations. However, the demographic models that have been inferred for maize and humans are quite different. Maize is inferred to have had a recent, major domestication bottleneck that was essentially instantaneous and followed by rapid exponential growth [59]. In contrast, demographic models for non-African humans suggest a much more distant bottleneck that was sustained over a

484 longer period of time, and only recently have non-African populations experienced ram-
485 pant growth (coinciding with the advent of agriculture). Given the vastly different demo-
486 graphic models of the two species, it is therefore not surprising that patterns of variation
487 would be different.

488 The greater contemporary N_e of non-Africans could theoretically result in a great-
489 er efficacy of purifying selection and, consequently, a stronger efficacy of BGS, leading
490 to their observed lower π/π_0 relative to Africans. However, it is very unlikely that this
491 explains the observed patterns of relative diversity that we see. The greater contempo-
492 rary population size of non-Africans has transpired only in the very recent past, with ac-
493 celerated growth in Europeans occurring within the last few hundred generations
494 [23,81–84]. Rather, our simulations indicate that the response of π in regions under
495 BGS is driven by the ancient, sustained population contractions humans have experi-
496 enced, with reductions in π/π_0 occurring concomitantly with the out-of-Africa bottleneck
497 and European-East Asian split bottleneck events (Fig 5) and continuing even after the
498 European and East Asian expansion events. In addition, our empirical measurements of
499 ψ/ψ_0 demonstrate that in recent time, BGS has had a lower effect in non-Africans com-
500 pared to Africans. Our simulations further corroborate this result. The greater sensitivity
501 of regions under BGS to population contractions and accelerated genetic drift is a more
502 likely explanation. Broadly, our results show that contemporary patterns of neutral di-
503 versity cannot easily be attributable to contemporary forces of selection but instead may
504 be exhibiting signatures that are still dominated by older demographic events. Interest-
505 ingly though, our simulations reveal an additional factor that can influence the impact of
506 BGS within populations – migration between populations. We observe that the ex-

change of deleterious variants from populations that have experienced extensive bottlenecks to populations with a more stable demography can magnify the strength of selection at linked sites. In particular, our simulations show that both π/π_0 and ψ/ψ_0 decrease in Africans despite the fact that they are inferred to have been constant in size in their recent evolutionary history (Fig 5B). These patterns disappear when migration is removed (Fig S7, S12 Fig B), however more work is needed to definitively test this.

While we describe here the differential effects of non-equilibrium demography on neutral diversity in regions under strong and weak BGS, it is worth mentioning that differences in the reduction of neutral diversity in the genome between different populations have also been investigated at the level of entire chromosomes. In particular, analyses of neutral diversity comparing autosomes to non-autosomes (i.e., sex chromosomes and the mitochondrial genome [mtDNA]) have been conducted. Interestingly, these studies have shown that population contractions have impacted the relative reduction of neutral diversity between non-autosomes and autosomes in a similar fashion to what we have observed between regions of strong BGS and weak BGS, with the greatest losses occurring in bottlenecked populations. This was demonstrated in humans [85] and later modeled and shown in other species [86], with the explanation that stronger genetic drift due to the lower N_e of non-autosomes causes diversity to be lost more quickly in response to population size reductions. Recent work in humans has confirmed such predictions by showing that relative losses of neutral diversity in the non-autosomes are greatest for non-Africans [87–89]. These studies, plus others [90], have also shown that there is strong evidence for a more dominant effect of linked selection on the sex chromosomes relative to the autosomes in humans.

530 Since linked selection is a pervasive force in shaping patterns of diversity across
531 the genomes in a range of biological species [1], it has been provided as an argument
532 for why neutral diversity and estimates of N_e are relatively constrained across species in
533 spite of the large variance in census population sizes that exist [47,91]. However, since
534 population bottlenecks are common among species and have an inordinate influence on
535 N_e [20], demography has also been argued as a major culprit for constrained diversity
536 [2,91–93]. Yet, as we show in humans, it is likely that patterns of neutral diversity are in
537 fact jointly impacted by both of these forces, magnifying one another to deplete levels of
538 diversity beyond what is expected by either one independently. This may play an even
539 larger role in higher N_e species such as *Drosophila*, where the overall distribution of B
540 was inferred to be even smaller (i.e., exhibiting stronger BGS) than in humans [32]. In
541 our work, we also identify a potentially substantial role for migration from smaller popu-
542 lations that harbor more strongly deleterious alleles on patterns of linked neutral diversi-
543 ty in large populations. Together, these combined effects may help provide additional
544 clues for the puzzling lack of disparity in genetic diversity among different species [94].
545 Finally, our results also have implications for medical genetics research, since
546 selection may be acting on functional regions contributing to disease susceptibility.
547 Since different populations will have experienced different demographic histories, the
548 action of linked selection may result in disparate patterns of genetic variation (with ele-
549 vated levels of drift) near causal loci. Recent work has already demonstrated that BGS's
550 consequence of lowering diversity impacts power for disease association tests [95]. Our
551 results indicate that this impact may be even further exacerbated by demography in bot-
552 tlenecked populations, leading to potentially larger discrepancies in power between dif-

553 ferent populations. Overall, this should encourage further scrutiny for tests and SNP
554 panels optimized for one population since they may not be easily translatable to other
555 populations. It should also further motivate investigators to simultaneously account for
556 demography and linked selection when performing tests to uncover disease variants
557 within the genome [95–97].
558

559 ## Materials and methods

560 **Data**

561 2,504 samples from 26 populations in phase 3 of the Thousand Genomes Project
562 (TGP) [9] were downloaded from ftp://ftp.ncbi.nlm.nih.gov/1000genomes/. vcftools
563 (v0.1.12a) [98] and custom python scripts were used to gather all bi-allelic SNP sites
564 from the autosomes of the entire sample set.

565 A subset of TGP samples that were sequenced to high coverage (~45X) by
566 Complete Genomics (CG) were downloaded from
567 ftp://ftp.ncbi.nlm.nih.gov/1000genomes/. After filtering out related individuals via pedi-
568 gree analyses, we analyzed 53 YRI, 64 CEU, and 62 CHS samples (S2 Table). The
569 cgatools (v1.8.0) listvariants program was first used to gather all SNPs from the 179
570 samples using their CG ASM "Variations Files" (CG format version 2.2). Within each
571 population, the number of reference and alternate allele counts for each SNP was then
572 calculated using the cgatools testvariants program and custom python scripts. Only al-
573 lele counts across high quality sites (i.e., those classified as VQHIGH variant quality by
574 CG) were included. Low quality sites (i.e., those with VQLOW variant quality) were
575 treated as missing data. Only autosomes were kept. Non-bi-allelic SNPs and sites vio-

576 lating Hardy-Weinberg equilibrium (HWE) (p-value < 0.05 with a Bonferroni correction
577 for multiple SNP testing) were also removed.

578 We collected 13 whole-genome sequenced KhoeSan samples (sequence-
579 coverage: 2.5-50X, see S3 Table in Supporting information) from 3 studies [99–101]
580 and used the processed vcf files from each of those respective studies to gather all bi-
581 allelic polymorphic SNPs (i.e., the union of variants across all vcf files). SNPs were only
582 retained if they were polymorphic within the 13 samples (i.e., sites called as alternate
583 only within the sample set were ignored).

584

585 **Filtering and ascertainment scheme**

586 Positions in the genome were annotated for background selection by using the
587 background selection coefficient, *B*, which was inferred by McVicker et al. [6] and down-
588 loaded from http://www.phrap.org/othersoftware.html. *B* was inferred by applying a clas-
589 sical model of BGS [60], which treats its effects as a simple reduction in N_e at neutral
590 sites as a function of their recombination distance from conserved loci, the strength of
591 purifying selection at those conserved loci, and the deleterious mutation rate. *B* can be
592 interpreted as the reduced fraction of neutral genetic diversity at a particular site along
593 the genome that is caused by BGS, with a value of 0 indicating a near complete remov-
594 al of neutral genetic diversity due to BGS and a *B* value of 1 indicating little to no effect
595 of BGS on neutral genetic diversity ($B = \pi/\pi_0 = N_e/N_0$). Positions for *B* were lifted over
596 from hg18 to hg19 using the UCSC liftOver tool. Sites that failed to uniquely map from
597 hg18 to hg19 or failed to uniquely map in the reciprocal direction were excluded. Sites
598 lacking a *B* value were also ignored. We focused our analyses on those regions of the

599 genome within the top 1%, 5%, 10%, and 25% of the genome-wide distribution of *B* and
600 within the bottom 1% of the genome-wide distribution of *B*. These quantiles correspond
601 to the *B* values 0.095, 0.317, 0.463, 0.691, and 0.994, respectively.

602 A set of 13 filters (referred to as the "13-filter set") were used to limit errors from
603 sequencing and misalignments with rhesus macaque and to remove regions potentially
604 under the direct effects of natural selection and putative selective sweeps (we ignore
605 the linked selection effects of background selection). These filters were applied to all
606 samples in phase 3 TGP (all filters are in build hg19) for all sets of analyses (see S4
607 Table in Supporting information for the total number of Mb that passed the described
608 filters below for each particular *B* quantile):

609 1. Coverage/exome: For phase 3 data, regions of the genome that were part of
610 the high coverage exome were excluded (see
611 ftp://ftp.ncbi.nlm.nih.gov/1000genomes/ftp/technical/reference/exome_pull_do
612 wn_targets/20130108.exome.targets.bed.README). This was done to limit
613 biases due to differing levels of coverage across the genome and to remove
614 likely functional sites within the exome.
615 2. phyloP: Sites with phyloP [102] scores > 1.2 or < -1.2 were removed to limit
616 the effects of natural selection due to conservation or accelerated evolution.
617 Scores were downloaded from
618 http://hgdownload.cse.ucsc.edu/goldenPath/hg19/phyloP46way/.
619 3. phastCons: Regions in the UCSC conservation 46-way track (table:
620 phastCons46wayPlacental) [103] were removed to limit the effects of natural
621 selection due to conservation.

4. CpG: CpG islands in the UCSC CpG islands track were removed because of their potential role in gene regulation and/or being conserved.
5. ENCODE blacklist: Regions with high signal artifacts from next-generation sequencing experiments discovered during the ENCODE project [104] were removed.
6. Accessible genome mask: Regions not accessible to next-generation sequencing using short reads, according to the phase 3 TGP "strict" criteria, were removed (downloaded from ftp://ftp.ncbi.nlm.nih.gov/1000genomes/ftp/release/20130502/supporting/accessible_genome_masks/StrictMask/).
7. Simple repeats: Regions in the UCSC simple repeats track were removed due to potential misalignments with outgroups and/or being under natural selection.
8. Gaps/centromeres/telomeres: Regions in the UCSC gap track were removed, including centromeres and telomeres.
9. Segmental duplications: Regions in the UCSC segmental dups track [105] were removed to limit potential effects of natural selection and/or misalignments with rhesus macaque.
10. Transposons: Active transposons (HERVK retrotransposons, the AluY subfamily of Alu elements, SVA elements, and L1Ta/L1pre-Ta LINEs) in the human genome were removed.
11. Recent positive selection: Regions inferred to be under hard and soft selective sweeps (using iHS and iHH12 regions from selscan v1.2.0 [106]; S1 Ap-

645 pendix) within each phase 3 population were removed.

646 12. Non-coding transcripts: Non-coding transcripts from the UCSC genes track
647 were removed to limit potential effects of natural selection.

648 13. Synteny: Regions that did not share conserved synteny with rhesus macaque
649 (rheMac2) from UCSC syntenic net filtering were removed (downloaded from
650 http://hgdownload.soe.ucsc.edu/goldenPath/hg19/vsRheMac2/syntenicNet/).

651 Additionally, an extra set of filters was applied, but only for those estimates of diversity
652 that controlled for GC-biased gene conversion and recombination hotspots:

653 14. GC-biased gene conversion (gBGC): Regions in UCSC phastBias track [107]
654 from UCSC genome browser were removed to limit regions inferred to be un-
655 der strong GC-biased gene conversion.

656 15. Recombination hotspots: All sites within 1.5 kb (i.e., 3 kb windows) of sites
657 with recombination rates ≥ 10 cM/Mb in the 1000G OMNI genetic maps for
658 non-admixed populations (downloaded from ftp://ftp-
659 trace.ncbi.nih.gov/1000genomes/ftp/technical/working/20130507_omni_reco
660 mbination_rates/) and the HapMap II genetic map [108] were removed. 1.5 kb
661 flanking regions surrounding the center of hotspots identified by Ref. [109]
662 (downloaded from
663 http://science.sciencemag.org/content/sci/suppl/2014/11/12/346.6211.125644
664 2.DC1/1256442_DatafileS1.txt) were also removed, except for the cases in
665 which the entire hotspot site was greater than 3 kb in length (in which case
666 just the hotspot was removed).

667 To generate a set of four-fold degenerate synonymous sites, all polymorphic

668 sites that we retained from the high-coverage Complete Genomic samples were anno-
669 tated using the program ANNOVAR [110] with Gencode V19 annotations. ANNOVAR
670 and Gencode V19 annotations were also used to gather an autosome-wide set of four-
671 fold degenerate sites, resulting in 5,188,972 total sites.
672
673 **Demographic inference**
674 The inference tool dadi (v1.6.3) [7] was used to fit, via maximum likelihood, the 3-
675 population 13-parameter demographic model of Gutenkunst et al. [7] to the 179 YRI,
676 CEU, and CHS samples from the high coverage CG dataset of TGP. This sample set
677 consisted of 53 YRI (African), 64 CEU (European), and 62 CHS (East Asian) samples.
678 The demographic model incorporates an ancient human expansion in Africa and a sin-
679 gle out-of-Africa bottleneck followed by European- and East Asian-specific bottlenecks,
680 as well as exponential growth in both non-African populations and migration between
681 populations. During the inference procedure, each population was projected down to
682 106 chromosomes, corresponding to the maximum number of chromosomes available
683 in the CG YRI population. Sites were polarized with chimpanzee to identify putative an-
684 cestral/derived alleles using the chain and netted alignments of hg19 with panTro4
685 (http://hgdownload.soe.ucsc.edu/goldenPath/hg19/vsPanTro4/axtNet/), and the correc-
686 tion for ancestral misidentification [111] option in dadi was used. The 13-filter set de-
687 scribed previously was applied to the CG data set, and an additional filter keeping only
688 the autosomal sites in the top 1% of B ($B \geq 0.994$) was also applied in order to mitigate
689 potential biases in inference due to BGS [52,65] or other forms of linked selection [51].
690 After site filtering and correction for ancestral misidentification, a total of 110,582 segre-

691 gating sites were utilized by dadi for the inference procedure. For optimization, grid
692 points of 120, 130, and 140 were used, and 15 independent optimization runs were
693 conducted from different initial parameter points to ensure convergence upon a global
694 optimum. An effective sequence length (L) of 7.15 Mb was calculated from the input se-
695 quence data after accounting for the fraction of total sites removed due to filtering. In
696 addition to the 13-filter set, this filtering included sites violating HWE, sites without B
697 value information, sites that did not have at least 106 sampled chromosomes in each
698 population, sites with more than two alleles, sites that did not have tri-nucleotide infor-
699 mation for the correction for ancestral misidentification step, and sites treated as miss-
700 ing data. For calculating the reference effective population size, a mutation rate (μ) of
701 1.66 x 10^{-8} (inferred from Ref. [112]) was used. Using the optimized θ from dadi after
702 parameter fitting, the equation $\theta = 4N_e\mu L$ was solved for N_e to generate the reference
703 effective population size, from which all other population N_e's were calculated. This
704 same procedure was also used to infer demographic parameters from four-fold degen-
705 erate synonymous sites across the same set of samples. After site filtering (note that B
706 and the 13-filter set were not included in the filtering step for four-fold degenerate syn-
707 onymous sites), 41,260 segregating sites were utilized by dadi for the inference proce-
708 dure, and an effective sequence length of 2.37 Mb was used for calculating the refer-
709 ence effective population size.
710
711 **Simulations**
712 Forward simulations incorporating the results from the demographic inference
713 procedure described above and a model of background selection were conducted using

714 SFS_CODE [113]. For the model of background selection, the recombination rate, ρ,
715 and the fraction of the genome experiencing deleterious mutation were calculated using
716 the 2 Mb region of chr3: 48,600,000-50,600,000, which has been subject to the strong-
717 est amount of BGS in the human genome (mean B = 0.002). A population-scaled re-
718 combination rate (ρ) of 6.0443 x 10^{-5} was calculated for this region using the HapMap II
719 GRCh37 genetic map [108]. For ascertaining the fraction of sites experiencing deleteri-
720 ous mutation, the number of non-coding "functional" sites in this region was first calcu-
721 lated by taking the union of all phastCons sites and phyloP sites with scores > 1.2 (indi-
722 cating conservation) that did not intersect with any coding exons. This amount totaled to
723 270,348 base pairs. Additionally, the number of coding sites was calculated by summing
724 all coding exons within this region from GENCODE v19, which totaled to 138,923 base
725 pairs. From these totals, the total fraction of deleterious sites, 0.2046, was generated.
726 The background selection model was simulated using a middle 30 kb neutral re-
727 gion flanked by two 1 Mb regions under purifying selection. From the calculated fraction
728 of deleterious sites described above, 20.46% of sites in the two 1 Mb flanking regions
729 were simulated as being deleterious. The mutation rate in our simulations for the delete-
730 rious sites and for neutral sites were both set to 1.66 x 10^{-8} [112]. Two distributions of
731 fitness effects were used for the deleterious sites, with 66.06% of deleterious sites using
732 the gamma distribution of fitness effects inferred across conserved non-coding regions
733 by Ref. [114] (β = 0.0415, α = 0.00515625) and 33.94% of deleterious sites using the
734 gamma distribution of fitness effects inferred across coding regions by Ref. [5] (β =
735 0.184, α = 0.00040244). The relative number of non-coding "functional" sites and coding
736 exons described above determined the relative number of sites receiving each distribu-

737 tion of fitness effects in our simulations. Gamma distribution parameters were scaled to
738 the ancestral population size of the demographic models used in Refs. [5,114]. An ex-
739 ample of the SFS_CODE command for our simulations is in S1 Supporting information.
740 To simulate varying levels of background selection strength, different total fractions of
741 our original calculated deleterious fraction of 0.2046 were used (i.e., 5%, 10%, 25%,
742 50%, and 100% of 0.2046). However, the same relative percentage of non-coding and
743 coding sites and mutation rate were used. These different simulated fractions of delete-
744 rious sites resulted in a reduced total deleterious mutation rate, *U*, which is the product
745 of the per-site deleterious mutation rate and the total number of sites experiencing dele-
746 terious mutation [66]. Thus, weaker effects of BGS were simulated. To simulate only the
747 effects of demography without background selection, only the 30 kb neutral region was
748 simulated. 2,000 independent simulations were conducted for each particular set of the
749 deleterious site fraction (2,000 x 6 = 12,000 total). Simulations output population genetic
750 information every 100 generations and also at each generation experiencing a popula-
751 tion size change (22,117 total generations were simulated), from which mean pairwise
752 nucleotide diversity (π) and singleton density (ψ) was calculated across the 2,000 simu-
753 lations.
754

755 **Population-specific calculations of diversity and singleton density**

756 Mean pairwise genetic diversity (π) and singleton density (ψ) was calculated as a
757 function of the *B* quantile bins described in “Filtering and ascertainment scheme” for
758 each of the 20 non-admixed populations in phase 3 TGP and, for π, across 4 broad
759 populations that grouped the 20 non-admixed populations together by continent (Afri-

760 can, European, South Asian, and East Asian, see S12 Table in Supporting information).
761 Additionally, only regions of the genome passing the 13-filter set were used in the calcu-
762 lations of π and ψ (see S4 Table in Supporting information for total number of Mb used
763 in diversity calculations for each *B* quantile). When calculating ψ for each non-admixed
764 phase 3 TGP population, the site-frequency spectrum was first projected down to 2N =
765 170 samples (the number of chromosomes in MSL, the smallest phase 3 population
766 sample) using a hypergeometric distribution [7] from each population's full site-
767 frequency spectrum. This allowed for unbiased comparisons of singleton density be-
768 tween all populations. For estimates of diversity controlling for gBGC or recombination
769 hotspots, the additional corresponding filters described in "Filtering and ascertainment
770 scheme" were also used. Only 100 kb regions of the genome with at least 10 kb of di-
771 vergence information with Rhesus macaque were used in π and ψ calculations (see
772 "Normalization of diversity and divergence calculations with Rhesus macaque" below).
773

774 **Normalization of diversity/singleton density and divergence calculations with**
775 **Rhesus macaque**

776 To calculate human divergence with Rhesus macaque, we downloaded the
777 syntenic net alignments between hg19 and rheMac2 that were generated by blastz from
778 http://hgdownload.cse.ucsc.edu/goldenpath/hg19/vsRheMac2/syntenicNet/. We binned
779 the human genome into non-overlapping 100 kb bins and calculated divergence within
780 each bin by taking the proportion of base pair differences between human and Rhesus
781 macaque. Gaps between human and Rhesus macaque, positions lacking alignment in-
782 formation, and positions that did not pass the 13-filter set described in "Filtering and

783 ascertainment scheme" were ignored in the divergence estimate. Additionally, a sepa-
784 rate set of divergence estimates were also made using the additional set of filtering cri-
785 teria that removed those regions under gBGC or in recombination hotspots and were
786 used for normalizing diversity in those measurements that controlled for gBGC and
787 hotspots.

788 When normalizing diversity and singleton density by divergence, only 100 kb bins
789 that had at least 10 kb of divergence information were used (21,100 bins total for 13-
790 filter set, 20,935 bins total for the 13-filter set plus the additional gBGC and hotspot fil-
791 ters). Bins with less than 10 kb of divergence information were ignored. To make esti-
792 mates comparable, in those measurements of diversity that did not normalize by diver-
793 gence, diversity was still calculated using the same set of 100 kb bins that had at least
794 10 kb for estimating divergence.

795

796 **Calculations of population differentiation (F_{ST}) and linear regression**

797 F_{ST} calculations were performed as a function of B between every pair of non-
798 admixed phase 3 TGP populations not belonging to the same continental group (150
799 pairs total). We followed the recommendations in Bhatia et al. [63] to limit biases in F_{ST}
800 due to 1) type of estimator used, 2) averaging over SNPs, and 3) SNP ascertainment.
801 Specifically, we 1) used the Hudson-based F_{ST} estimator [115], 2) used a ratio of
802 averages for combining F_{ST} estimated across different SNPs, and 3) ascertained SNPs
803 based on being polymorphic in an outgroup (i.e., the KhoeSan). For ascertaining SNPs
804 in the KhoeSan, we also performed filtering according to the filtering scheme described
805 under "Filtering and ascertainment scheme." For a position to be considered

806 polymorphic in the KhoeSan, at least one alternate allele and one reference allele had
807 to be called across the 13 genomes we utilized (see "Data"). These criteria left
808 3,497,105 total sites in the genome in the phase 3 dataset for F_{ST} to be estimated
809 across.

810 F_{ST} was calculated across 2% quantile bins of B (based on the genome-wide
811 distribution of B) for all pairwise comparisons of populations between a specific pair of
812 continental groups (25 pairs total) or across all pairwise comparisons using all continen-
813 tal groups (150 pairs total). Simple linear regression was performed with the model F_{ST}
814 $= \beta_0 + \beta_1 B + \varepsilon$. The mean of the bounds defining each quantile bin was used when de-
815 fining the explanatory variables for the regression. Linear regression, robust linear re-
816 gression [64], and simple correlation were performed using the lm(), rlm(), and cor()
817 functions, respectively, in the R programming language (www. r-project.org). To gener-
818 ate standard errors of the mean, this same procedure was performed on F_{ST} results
819 generated from each of 1,000 bootstrapped iterations of the data.

820

821 **Bootstrapping**

822 **Diversity Estimates.** To control for the structure of linkage disequilibrium and correla-
823 tion between SNPs along the genome, we partitioned the human genome into non-
824 overlapping 100 kb bins (these bins were identical to the 100 kb bins used for estimat-
825 ing divergence) and calculated mean pairwise diversity (π) or heterozygosity within each
826 bin. We also normalized the diversity estimates by divergence within each bin. We then
827 bootstrapped individual genomes by sampling, with replacement, the 100 kb bins until
828 the number of sampled bins equaled the number of bins used for calculating the diversi-

ty point estimates (i.e., 21,100 bins or 20,935 bins total, depending on whether filters for gBGC and hotspots were applied). 1,000 total bootstrap iterations were completed and standard errors of the mean were calculated by taking the standard deviation from the resulting bootstrap distribution.

***F_{ST}*.** For bootstrapping F_{ST}, the human genome was partitioned into non-overlapping 100 kb bins and were sampled with replacement until 28,823 bins were selected (the total number of non-overlapping 100 kb bins in the human autosomes). F_{ST} was then calculated genome-wide for the bootstrapped genome as a function of *B* for every pair-wise comparison of non-admixed phase 3 TGP populations not belonging to the same continental group. 1,000 total bootstrap iterations were completed and standard errors of the mean were calculated by taking the standard deviation from the F_{ST} distribution calculated from all 1,000 iterations.

Acknowledgements

We thank Lawrence Uricchio, Dominic Tong, Melissa Spear, Nicolas Strauli and three anonymous reviewers for helpful comments on the manuscript. The computations in this paper were run on the QB3 Shared Cluster at the University of California, San Francisco.

References

1. Cutter AD, Payseur BA. Genomic signatures of selection at linked sites: unifying the disparity among species. Nat Rev Genet. 2013;14: 262–274. doi:10.1038/nrg3425
2. Ellegren H, Galtier N. Determinants of genetic diversity. Nat Rev Genet. 2016;17: 422–433. doi:10.1038/nrg.2016.58
3. Sabeti PC, Reich DE, Higgins JM, Levine HZP, Richter DJ, Schaffner SF, et al.

855 Detecting recent positive selection in the human genome from haplotype
856 structure. Nature. 2002;419: 832–837. doi:10.1038/nature01027.1.
857 4. Williamson SH, Hernandez R, Fledel-Alon A, Zhu L, Nielsen R, Bustamante CD.
858 Simultaneous inference of selection and population growth from patterns of
859 variation in the human genome. Proc Natl Acad Sci. 2005;102: 7882–7887.
860 doi:10.1073/pnas.0502300102
861 5. Boyko AR, Williamson SH, Indap AR, Degenhardt JD, Hernandez RD, Lohmueller
862 KE, et al. Assessing the evolutionary impact of amino acid mutations in the
863 human genome. PLoS Genet. 2008;4: e1000083.
864 doi:10.1371/journal.pgen.1000083
865 6. McVicker G, Gordon D, Davis C, Green P. Widespread genomic signatures of
866 natural selection in hominid evolution. PLoS Genet. 2009;5: e1000471.
867 doi:10.1371/journal.pgen.1000471
868 7. Gutenkunst RN, Hernandez RD, Williamson SH, Bustamante CD. Inferring the
869 joint demographic history of multiple populations from multidimensional SNP
870 frequency data. PLoS Genet. 2009;5: e1000695.
871 doi:10.1371/journal.pgen.1000695
872 8. Li H, Durbin R. Inference of human population history from individual whole-
873 genome sequences. Nature. 2011;475: 493–496. doi:10.1038/nature10231
874 9. Auton A, Abecasis GR, Altshuler DM, Durbin RM, Abecasis GR, Bentley DR, et al.
875 A global reference for human genetic variation. Nature. 2015;526: 68–74.
876 doi:10.1038/nature15393
877 10. Lack JB, Lange JD, Tang AD, Corbett-Detig RB, Pool JE. A thousand fly
878 genomes: An expanded Drosophila genome nexus. Mol Biol Evol. 2016;33: 3308–
879 3313. doi:10.1093/molbev/msw195
880 11. Gibbs RA, Taylor JF, Van Tassell CP, Barendse W, Eversole KA, Gill CA, et al.
881 Genome-wide survey of SNP variation uncovers the genetic structure of cattle
882 breeds. Science. 2009;324: 528–532. doi:10.1126/science.1167936
883 12. Marsden CD, Ortega-Del Vecchyo D, O'Brien DP, Taylor JF, Ramirez O, Vilà C,
884 et al. Bottlenecks and selective sweeps during domestication have increased
885 deleterious genetic variation in dogs. Proc Natl Acad Sci. 2016;113: 152–157.
886 doi:10.1073/pnas.1512501113
887 13. Caicedo AL, Williamson SH, Hernandez RD, Boyko A, Fledel-Alon A, York TL, et
888 al. Genome-wide patterns of nucleotide polymorphism in domesticated rice. PLoS
889 Genet. 2007;3: 1745–1756. doi:10.1371/journal.pgen.0030163
890 14. Begun DJ, Aquadro CF. African and North American populations of Drosophila
891 melanogaster are very different at the DNA level. Nature. 1993;365: 548–550.
892 doi:10.1038/365548a0
893 15. Haddrill PR, Thornton KR, Charlesworth B, Andolfatto P. Multilocus patterns of
894 nucleotide variability and the demographic and selection history of Drosophila
895 melanogaster populations. Genome Res. 2005;15: 790–799.
896 doi:10.1101/gr.3541005
897 16. Ometto L, Glinka S, De Lorenzo D, Stephan W. Inferring the effects of
898 demography and selection on Drosophila melanogaster populations from a
899 chromosome-wide scan of DNA variation. Mol Biol Evol. 2005;22: 2119–2130.
900 doi:10.1093/molbev/msi207

17. Hernandez RD, Hubisz MJ, Wheeler DA, Smith DG, Ferguson B, Rogers J, et al. Demographic histories and patterns of linkage disequilibrium in Chinese and Indian rhesus macaques. Science. 2007;316: 240–243. doi:10.1126/science.1140462
18. Ramachandran S, Deshpande O, Roseman CC, Rosenberg NA, Feldman MW, Cavalli-Sforza LL. Support from the relationship of genetic and geographic distance in human populations for a serial founder effect originating in Africa. Proc Natl Acad Sci. 2005;102: 15942–15947. doi:10.1073/pnas.0507611102
19. Henn BM, Cavalli-Sforza LL, Feldman MW. The great human expansion. Proc Natl Acad Sci. 2012;109: 17758–17764. doi:10.1073/pnas.1212380109
20. Charlesworth B. Effective population size and patterns of molecular evolution and variation. Nat Rev Genet. 2009;10: 195–205. doi:10.1038/nrg2526
21. Nei M, Maruyama T, Chakraborty R. The bottleneck effect and genetic variability in populations. Evolution (N Y). 1975;29: 1–10. doi:10.2307/2407137
22. Gravel S, Henn BM, Gutenkunst RN, Indap AR, Marth GT, Clark AG, et al. Demographic history and rare allele sharing among human populations. Proc Natl Acad Sci. 2011;108: 11983–11988. doi:10.1073/pnas.1019276108
23. Tennessen JA, Bigham AW, O'Connor TD, Fu W, Kenny EE, Gravel S, et al. Evolution and functional impact of rare coding variation from deep sequencing of human exomes. Science. 2012;337: 64–69. doi:10.1126/science.1219240
24. Charlesworth D. Balancing selection and its effects on sequences in nearby genome regions. PLoS Genet. 2006;2: 379–384. doi:10.1371/journal.pgen.0020064
25. Maynard Smith J, Haigh J. The hitch-hiking effect of a favourable gene. Genet Res. 1974;23: 23–35. doi:10.1017/S0016672308009579
26. Charlesworth B, Morgan MT, Charlesworth D. The effect of deleterious mutations on neutral molecular variation. Genetics. 1993;134: 1289–1303.
27. Kim Y, Stephan W. Joint effects of genetic hitchhiking and background selection on neutral variation. Genetics. 2000;155: 1415–1427.
28. Begun DJ, Aquadro CF. Levels of naturally occurring DNA polymorphism correlate with recombination rates in D. melanogaster. Nature. 1992;356: 519–520. doi:10.1038/356519a0
29. Charlesworth B. Background selection and patterns of genetic diversity in Drosophila melanogaster. Genet Res. 1996;68: 131–149. doi:10.1017/S0016672300034029
30. Andolfatto P. Hitchhiking effects of recurrent beneficial amino acid substitutions in the Drosophila melanogaster genome. Genome Res. 2007;17: 1755–1762. doi:10.1101/gr.6691007
31. Sella G, Petrov DA, Przeworski M, Andolfatto P. Pervasive natural selection in the Drosophila genome? PLoS Genet. 2009;5: e1000495. doi:10.1371/journal.pgen.1000495
32. Comeron JM. Background selection as baseline for nucleotide variation across the drosophila genome. PLoS Genet. 2014;10: e1004434. doi:10.1371/journal.pgen.1004434
33. Elyashiv E, Sattath S, Hu TT, Strutsovsky A, McVicker G, Andolfatto P, et al. A genomic map of the effects of linked selection in Drosophila. PLoS Genet.

947 2016;12: e1006130. doi:10.1371/journal.pgen.1006130
948 34. Flowers JM, Molina J, Rubinstein S, Huang P, Schaal BA, Purugganan MD.
949 Natural selection in gene-dense regions shapes the genomic pattern of
950 polymorphism in wild and domesticated rice. Mol Biol Evol. 2012;29: 675–687.
951 doi:10.1093/molbev/msr225
952 35. Xu X, Liu X, Ge S, Jensen JD, Hu F, Li X, et al. Resequencing 50 accessions of
953 cultivated and wild rice yields markers for identifying agronomically important
954 genes. Nat Biotechnol. 2012;30: 105–111. doi:10.1038/nbt.2050
955 36. Andersen EC, Gerke JP, Shapiro JA, Crissman JR, Ghosh R, Bloom JS, et al.
956 Chromosome-scale selective sweeps shape Caenorhabditis elegans genomic
957 diversity. Nat Genet. 2012;44: 285–290. doi:10.1038/ng.1050
958 37. Cutter AD, Payseur BA. Selection at linked sites in the partial selfer
959 Caenorhabditis elegans. Mol Biol Evol. 2003;20: 665–673.
960 doi:10.1093/molbev/msg072
961 38. Reed FA, Akey JM, Aquadro CF. Fitting background-selection predictions to
962 levels of nucleotide variation and divergence along the human autosomes.
963 Genome Res. 2005;15: 1211–1221. doi:10.1101/gr.3413205
964 39. Voight BF, Kudaravalli S, Wen X, Pritchard JK. A map of recent positive selection
965 in the human genome. PLoS Biol. 2006;4: 0446–0458.
966 doi:10.1371/journal.pbio.0040072
967 40. Cai JJ, Macpherson JM, Sella G, Petrov DA. Pervasive hitchhiking at coding and
968 regulatory sites in humans. PLoS Genet. 2009;5: e1000336.
969 doi:10.1371/journal.pgen.1000336
970 41. Hernandez RD, Kelley JL, Elyashiv E, Melton SC, Auton A, McVean G, et al.
971 Classic selective sweeps were rare in recent human evolution. Science.
972 2011;331: 920–924. doi:10.1126/science.1198878
973 42. Lohmueller KE, Albrechtsen A, Li Y, Kim SY, Korneliussen T, Vinckenbosch N, et
974 al. Natural selection affects multiple aspects of genetic variation at putatively
975 neutral sites across the human genome. PLoS Genet. 2011;7: e1002326.
976 doi:10.1371/journal.pgen.1002326
977 43. Alves I, Šrámková Hanulová A, Foll M, Excoffier L. Genomic data reveal a
978 complex making of humans. PLoS Genet. 2012;8: e1002837.
979 doi:10.1371/journal.pgen.1002837
980 44. Granka JM, Henn BM, Gignoux CR, Kidd JM, Bustamante CD, Feldman MW.
981 Limited evidence for classic selective sweeps in African populations. Genetics.
982 2012;192: 1049–1064. doi:10.1534/genetics.112.144071
983 45. Enard D, Messer PW, Petrov DA. Genome-wide signals of positive selection in
984 human evolution. Genome Res. 2014;24: 885–895. doi:10.1101/gr.164822.113
985 46. Bank C, Ewing GB, Ferrer-Admettla A, Foll M, Jensen JD. Thinking too positive?
986 Revisiting current methods of population genetic selection inference. Trends
987 Genet. 2014;30: 540–546. doi:10.1016/j.tig.2014.09.010
988 47. Corbett-Detig RB, Hartl DL, Sackton TB. Natural selection constrains neutral
989 diversity across a wide range of species. PLoS Biol. 2015;13: e1002112.
990 doi:10.1371/journal.pbio.1002112
991 48. Comeron JM. Background selection as null hypothesis in population genomics:
992 insights and challenges from Drosophila studies. Philos Trans R Soc B. 2017;372:

20160471. doi:10.1098/rstb.2016.0471
49. Zeng K. A coalescent model of background selection with recombination, demography and variation in selection coefficients. Heredity (Edinb). 2013;110: 363–371. doi:10.1038/hdy.2012.102
50. Nicolaisen LE, Desai MM. Distortions in genealogies due to purifying selection and recombination. Genetics. 2013;195: 221–230. doi:10.1534/genetics.113.152983
51. Schrider DR, Shanku AG, Kern AD. Effects of linked selective sweeps on demographic inference and model selection. Genetics. 2016;204: 1207–1223. doi:10.1534/genetics.116.190223
52. Ewing GB, Jensen JD. The consequences of not accounting for background selection in demographic inference. Mol Ecol. 2016;25: 135–141. doi:10.1111/mec.13390
53. Pennings PS, Kryazhimskiy S, Wakeley J. Loss and recovery of genetic diversity in adapting populations of HIV. PLoS Genet. 2014;10: e1004000. doi:10.1371/journal.pgen.1004000
54. Brandvain Y, Wright SI. The limits of natural selection in a nonequilibrium world. Trends Genet. 2016;32: 201–210. doi:10.1016/j.tig.2016.01.004
55. Koch E, Novembre J. A temporal perspective on the interplay of demography and selection on deleterious variation in humans. G3. 2017;7: 1027–1037. doi:10.1534/g3.117.039651
56. Lohmueller KE, Indap AR, Schmidt S, Boyko AR, Hernandez RD, Hubisz MJ, et al. Proportionally more deleterious genetic variation in European than in African populations. Nature. 2008;451: 994–997. doi:10.1038/nature06611
57. Casals F, Hodgkinson A, Hussin J, Idaghdour Y, Bruat V, de Maillard T, et al. Whole-exome sequencing reveals a rapid change in the frequency of rare functional variants in a founding population of humans. PLoS Genet. 2013;9: e1003815. doi:10.1371/journal.pgen.1003815
58. Simons YB, Sella G. The impact of recent population history on the deleterious mutation load in humans and close evolutionary relatives. Curr Opin Genet Dev. 2016;41: 150–158. doi:10.1016/j.gde.2016.09.006
59. Beissinger TM, Wang L, Crosby K, Durvasula A, Hufford MB, Ross-Ibarra J. Recent demography drives changes in linked selection across the maize genome. Nat Plants. 2016;2: 16084. doi:10.1038/nplants.2016.84
60. Nordborg M, Charlesworth B, Charlesworth D. The effect of recombination on background selection. Genet Res. 1996;67: 159–174. doi:10.1017/S0016672300033619
61. Charlesworth B, Nordborg M, Charlesworth D. The effects of local selection, balanced polymorphism and background selection on equilibrium patterns of genetic diversity in subdivided populations. Genet Res. 1997;70: 155–174. doi:10.1017/S0016672397002954
62. Hu XS, He F. Background selection and population differentiation. J Theor Biol. 2005;235: 207–219. doi:10.1016/j.jtbi.2005.01.004
63. Bhatia G, Patterson N, Sankararaman S, Price AL. Estimating and interpreting FST: The impact of rare variants. Genome Res. 2013;23: 1514–1521. doi:10.1101/gr.154831.113

1039 64. Yu C, Yao W. Robust linear regression: A review and comparison. Commun Stat -
1040 Simul Comput. 2017;46: 6261–6282. doi:10.1080/03610918.2016.1202271
1041 65. Messer PW, Petrov DA. Frequent adaptation and the McDonald-Kreitman test.
1042 Proc Natl Acad Sci. 2013;110: 8615–8620. doi:10.1073/pnas.1220835110
1043 66. Charlesworth B. The effects of deleterious mutations on evolution at linked sites.
1044 Genetics. 2012;190: 5–22. doi:10.1534/genetics.111.134288
1045 67. Phung TN, Huber CD, Lohmueller KE. Determining the effect of natural selection
1046 on linked neutral divergence across species. PLoS Genet. 2016;12: e1006199.
1047 doi:10.1371/journal.pgen.1006199
1048 68. Burgess R, Yang Z. Estimation of hominoid ancestral population sizes under
1049 Bayesian coalescent models incorporating mutation rate variation and sequencing
1050 errors. Mol Biol Evol. 2008;25: 1979–1994. doi:10.1093/molbev/msn148
1051 69. Campos JL, Zhao L, Charlesworth B. Estimating the parameters of background
1052 selection and selective sweeps in Drosophila in the presence of gene conversion.
1053 Proc Natl Acad Sci. 2017;114: E4762–E4771. doi:10.1073/pnas.1619434114
1054 70. Eyre-Walker A, Keightley PD. Estimating the rate of adaptive molecular evolution
1055 in the presence of slightly deleterious mutations and population size change. Mol
1056 Biol Evol. 2009;26: 2097–2108. doi:10.1093/molbev/msp119
1057 71. Galtier N. Adaptive protein evolution in animals and the effective population size
1058 hypothesis. PLoS Genet. 2016;12: e1005774. doi:10.1371/journal.pgen.1005774
1059 72. Lim ET, Würtz P, Havulinna AS, Palta P, Tukiainen T, Rehnström K, et al.
1060 Distribution and medical impact of loss-of-function variants in the Finnish founder
1061 population. PLoS Genet. 2014;10: e1004494. doi:10.1371/journal.pgen.1004494
1062 73. Cao J, Schneeberger K, Ossowski S, Günther T, Bender S, Fitz J, et al. Whole-
1063 genome sequencing of multiple Arabidopsis thaliana populations. Nat Genet.
1064 2011;43: 956–963. doi:10.1038/ng.911
1065 74. Renaut S, Rieseberg LH. The accumulation of deleterious mutations as a
1066 consequence of domestication and improvement in sunflowers and other
1067 compositae crops. Mol Biol Evol. 2015;32: 2273–2283.
1068 doi:10.1093/molbev/msv106
1069 75. Balick DJ, Do R, Cassa CA, Reich D, Sunyaev SR. Dominance of deleterious
1070 alleles controls the response to a population bottleneck. PLoS Genet. 2015;11:
1071 e1005436. doi:10.1371/journal.pgen.1005436
1072 76. Do R, Balick D, Li H, Adzhubei I, Sunyaev S, Reich D. No evidence that selection
1073 has been less effective at removing deleterious mutations in Europeans than in
1074 Africans. Nat Genet. 2015;47: 126–131. doi:10.1038/ng.3186
1075 77. Simons YB, Turchin MC, Pritchard JK, Sella G. The deleterious mutation load is
1076 insensitive to recent population history. Nat Genet. 2014;46: 220–224.
1077 doi:10.1038/ng.2896
1078 78. Gravel S. When is selection effective? Genetics. 2016;203: 451–462.
1079 doi:10.1534/genetics.115.184630
1080 79. Braverman JM, Hudson RR, Kaplan NL, Langley CH, Stephan W. The hitchhiking
1081 effect on the site frequency spectrum of DNA polymorphisms. Genetics.
1082 1995;140: 783–796.
1083 80. Stephan W. Genetic hitchhiking versus background selection: the controversy and
1084 its implications. Philos Trans R Soc B. 2010;365: 1245–1253.

1085 doi:10.1098/rstb.2009.0278
1086 81. Coventry A, Bull-Otterson LM, Liu X, Clark AG, Maxwell TJ, Crosby J, et al. Deep
1087 resequencing reveals excess rare recent variants consistent with explosive
1088 population growth. Nat Commun. 2010;1: 131. doi:10.1038/ncomms1130
1089 82. Keinan A, Clark AG. Recent explosive human population growth has resulted in
1090 an excess of rare genetic variants. Science. 2012;336: 740–743.
1091 doi:10.1126/science.1217283
1092 83. Nelson MR, Wegmann D, Ehm MG, Kessner D, St. Jean P, Verzilli C, et al. An
1093 abundance of rare functional variants in 202 drug target genes sequenced in
1094 14,002 people. Science. 2012;337: 100–104. doi:10.1126/science.1217876
1095 84. Gazave E, Ma L, Chang D, Coventry A, Gao F, Muzny D, et al. Neutral genomic
1096 regions refine models of recent rapid human population growth. Proc Natl Acad
1097 Sci. 2014;111: 757–762. doi:10.1073/pnas.1310398110
1098 85. Fay JC, Wu CI. A human population bottleneck can account for the discordance
1099 between patterns of mitochondrial versus nuclear DNA variation. Mol Biol Evol.
1100 1999;16: 1003–1005. doi:10.1093/oxfordjournals.molbev.a026175
1101 86. Pool JE, Nielsen R. Population size changes reshape genomic patterns of
1102 diversity. Evolution (N Y). 2007;61: 3001–3006. doi:10.1111/j.1558-
1103 5646.2007.00238.x
1104 87. Gottipati S, Arbiza L, Siepel A, Clark AG, Keinan A. Analyses of X-linked and
1105 autosomal genetic variation in population-scale whole genome sequencing. Nat
1106 Genet. 2011;43: 741–743. doi:10.1038/ng.877
1107 88. Arbiza L, Gottipati S, Siepel A, Keinan A. Contrasting X-linked and autosomal
1108 diversity across 14 human populations. Am J Hum Genet. 2014;94: 827–844.
1109 doi:10.1016/j.ajhg.2014.04.011
1110 89. Wilson Sayres MA, Lohmueller KE, Nielsen R. Natural selection reduced diversity
1111 on human Y chromosomes. PLoS Genet. 2014;10: e1004064.
1112 doi:10.1371/journal.pgen.1004064
1113 90. Hammer MF, Woerner AE, Mendez FL, Watkins JC, Cox MP, Wall JD. The ratio
1114 of human X chromosome to autosome diversity is positively correlated with
1115 genetic distance from genes. Nat Genet. 2010;42: 830–831. doi:10.1038/ng.651
1116 91. Leffler EM, Bullaughey K, Matute DR, Meyer WK, Ségurel L, Venkat A, et al.
1117 Revisiting an old riddle: What determines genetic diversity levels within species?
1118 PLoS Biol. 2012;10: e1001388. doi:10.1371/journal.pbio.1001388
1119 92. Vucetich JA, Waite TA, Nunney L. Fluctuating population size and the ratio of
1120 effective to census population size. Evolution (N Y). 1997;51: 2017–2021.
1121 doi:10.2307/2411022
1122 93. Coop G. Does linked selection explain the narrow range of genetic diversity
1123 across species? bioRxiv. 2016; doi:10.1101/042598
1124 94. Lewontin RC. The genetic basis of evolutionary change. New York and London:
1125 Columbia University Press; 1974.
1126 95. Uricchio LH, Torres R, Witte JS, Hernandez RD. Population genetic simulations of
1127 complex phenotypes with implications for rare variant association tests. Genet
1128 Epidemiol. 2015;39: 35–44. doi:10.1002/gepi.21866
1129 96. Maher MC, Uricchio LH, Torgerson DG, Hernandez RD. Population genetics of
1130 rare variants and complex diseases. Hum Hered. 2012;74: 118–128.

1131 doi:10.1159/000346826
1132 97. Uricchio LH, Zaitlen NA, Ye CJ, Witte JS, Hernandez RD. Selection and explosive
1133 growth alter genetic architecture and hamper the detection of causal rare variants.
1134 Genome Res. 2016;26: 863–873. doi:10.1101/gr.202440.115
1135 98. Danecek P, Auton A, Abecasis G, Albers CA, Banks E, DePristo MA, et al. The
1136 variant call format and VCFtools. Bioinformatics. 2011;27: 2156–2158.
1137 doi:10.1093/bioinformatics/btr330
1138 99. Henn BM, Botigué LR, Peischl S, Dupanloup I, Lipatov M, Maples BK, et al.
1139 Distance from sub-Saharan Africa predicts mutational load in diverse human
1140 genomes. Proc Natl Acad Sci. 2016;113: E440-449.
1141 doi:10.1073/pnas.1510805112
1142 100. Kidd JM, Sharpton TJ, Bobo D, Norman PJ, Martin AR, Carpenter ML, et al.
1143 Exome capture from saliva produces high quality genomic and metagenomic
1144 data. BMC Genomics. 2014;15: 262. doi:10.1186/1471-2164-15-262
1145 101. Kim HL, Ratan A, Perry GH, Montenegro A, Miller W, Schuster SC. Khoisan
1146 hunter-gatherers have been the largest population throughout most of modern-
1147 human demographic history. Nat Commun. 2014;5: 5692.
1148 doi:10.1038/ncomms6692
1149 102. Pollard KS, Hubisz MJ, Rosenbloom KR, Siepel A. Detection of nonneutral
1150 substitution rates on mammalian phylogenies. Genome Res. 2010;20: 110–121.
1151 doi:10.1101/gr.097857.109
1152 103. Siepel A, Bejerano G, Pedersen JS, Hinrichs AS, Hou M, Rosenbloom K, et al.
1153 Evolutionarily conserved elements in vertebrate, insect, worm, and yeast
1154 genomes. Genome Res. 2005;15: 1034–1050. doi:10.1101/gr.3715005
1155 104. Bernstein BE, Birney E, Dunham I, Green ED, Gunter C, Snyder M, et al. An
1156 integrated encyclopedia of DNA elements in the human genome. Nature.
1157 2012;489: 57–74. doi:10.1038/nature11247
1158 105. Bailey JA, Yavor AM, Massa HF, Trask BJ, Eichler EE. Segmental duplications:
1159 Organization and impact within the current human genome project assembly.
1160 Genome Res. 2001;11: 1005–1017. doi:10.1101/gr.187101
1161 106. Szpiech ZA, Hernandez RD. selscan: An efficient multithreaded program to
1162 perform EHH-based scans for positive selection. Mol Biol Evol. 2014;31: 2824–
1163 2827. doi:10.1093/molbev/msu211
1164 107. Capra JA, Hubisz MJ, Kostka D, Pollard KS, Siepel A. A model-based analysis of
1165 GC-biased gene conversion in the human and chimpanzee genomes. PLoS
1166 Genet. 2013;9: e1003684. doi:10.1371/journal.pgen.1003684
1167 108. Frazer KA, Ballinger DG, Cox DR, Hinds DA, Stuve LL, Gibbs RA, et al. A second
1168 generation human haplotype map of over 3.1 million SNPs. Nature. 2007;449:
1169 851–861. doi:10.1038/nature06258
1170 109. Pratto F, Brick K, Khil P, Smagulova F, Petukhova G V, Camerini-Otero RD.
1171 Recombination initiation maps of individual human genomes. Science. 2014;346:
1172 1256442. doi:10.1126/science.1256442
1173 110. Wang K, Li M, Hakonarson H. ANNOVAR: Functional annotation of genetic
1174 variants from high-throughput sequencing data. Nucleic Acids Res. 2010;38:
1175 e164. doi:10.1093/nar/gkq603
1176 111. Hernandez RD, Williamson SH, Zhu L, Bustamante CD. Context-dependent

mutation rates may cause spurious signatures of a fixation bias favoring higher GC-content in humans. Mol Biol Evol. 2007;24: 2196–2202. doi:10.1093/molbev/msm149

112. Palamara PF, Francioli LC, Wilton PR, Genovese G, Gusev A, Finucane HK, et al. Leveraging distant relatedness to quantify human mutation and gene-conversion rates. Am J Hum Genet. 2015;97: 775–789. doi:10.1016/j.ajhg.2015.10.006

113. Hernandez RD. A flexible forward simulator for populations subject to selection and demography. Bioinformatics. 2008;24: 2786–2787. doi:10.1093/bioinformatics/btn522

114. Torgerson DG, Boyko AR, Hernandez RD, Indap A, Hu X, White TJ, et al. Evolutionary processes acting on candidate cis-regulatory regions in humans inferred from patterns of polymorphism and divergence. PLoS Genet. 2009;5: e1000592. doi:10.1371/journal.pgen.1000592

115. Hudson RR, Slatkin M, Maddison WP. Estimation of levels of gene flow from DNA sequence data. Genetics. 1992;132: 583–589.

Supporting information

S1 Appendix. Soft sweep detection and implementation in selscan v1.2.0.

S1 Supporting information.

S1 Fig. Inference models inferred from TGP CG high *B* neutral regions and coding four-fold degenerate sites. Solid lines are the inference results from running dadi on 53 YRI (African), 64 CEU (European), and 62 CHS (East Asian) TGP CG samples (projected down to 106 chromosomes during inference procedure) across neutral regions in the highest 1% *B* bin ($B \geq 0.994$). Broken lines represent the inference results using the same CG samples, but with sequence data only from coding four-fold degenerate synonymous sites.

S2 Fig. Diversity for TGP non-admixed populations while controlling for GC-biased gene conversion and recombination hotspots. (A) Normalized diversity (π/divergence) measured across the lowest 1% *B* quantile bin (strong BGS). (B) Normalized diversity measured across the highest 1% *B* quantile bin (weak BGS). (C) Rela-

1209 tive diversity: the ratio of normalized diversity for the lowest 1% *B* bin to normalized di-
1210 versity for the highest 1% *B* bin (π/π_0). Error bars represent ±1 SEM calculated from
1211 1,000 bootstrapped datasets.

1212 **S3 Fig. Diversity for TGP non-admixed populations without normalizing by diver-**
1213 **gence with Rhesus macaque.** (A) Diversity (π) measured across the lowest 1% *B*
1214 quantile bin (strong BGS). (B) Diversity measured across the highest 1% *B* quantile bin
1215 (weak BGS). (C) Relative diversity: the ratio of diversity for the lowest 1% *B* bin to diver-
1216 sity for the highest 1% *B* bin (π/π_0). Error bars represent ±1 SEM calculated from 1,000
1217 bootstrapped datasets.

1218 **S4 Fig. Diversity for TGP continental groups while controlling for GC-biased gene**
1219 **conversion and recombination hotspots.** (A) Normalized diversity (π/divergence)
1220 measured across the lowest 1%, 5%, 10% and 25% *B* quantile bins (strong BGS) and
1221 the highest 1% *B* quantile bin (weak BGS). (B) Relative diversity (π/π_0) for the lowest
1222 1%, 5%, 10%, and 25% *B* bins. Error bars represent ±1 SEM calculated from 1,000
1223 bootstrapped datasets.

1224 **S5 Fig. Diversity for TGP continental groups without normalizing by divergence**
1225 **with Rhesus macaque.** (A) Diversity (π) measured across the lowest 1%, 5%, 10% and
1226 25% *B* quantile bins (strong BGS) and the highest 1% *B* quantile bin (weak BGS). (B)
1227 Relative diversity (π/π_0) for the lowest 1%, 5%, 10%, and 25% *B* bins. Error bars repre-
1228 sent ±1 SEM calculated from 1,000 bootstrapped datasets.

1229 **S6 Fig. F_{ST} measured across joint bins of *B* and recombination rate for different**
1230 **TGP continental groups**. The left panels of S6 Figs A-E show F_{ST} measured as a func-
1231 tion of 25 4% recombination rate quantile bins conditional on three 2% *B* quantile bins

(note log scale of x-axis for recombination rate). The right panels of S6 Figs A-E show F_{ST} measured as a function of 25 4% *B* quantile bins conditional on three 2% recombination rate quantile bins. The following continental group comparisons are shown for each plot: (A) African vs. European, (B) African vs. East Asian, (C) European vs. South Asian, (D) European vs. East Asian, (E) South Asian vs. East Asian. Smaller transparent points and lines show the F_{ST} estimates and corresponding lines of best fit (using linear regression) for each of the pairwise population comparisons within a particular pair of continental groups (25 comparisons total). Larger opaque points are mean F_{ST} estimates across all pairwise comparisons within a particular pair of continental groups (with bold lines showing their corresponding lines of best fit).

S7 Fig. Simulations of diversity and relative diversity under BGS using a human demographic model without migration. (A) Inferred demographic model from Complete Genomics TGP data. The demographic model used for the simulations in S7 Fig are identical to those used for Fig 5, except that migration parameters between all populations are set to 0. (B) Simulated diversity at neutral sites across populations as a function of time under our inferred demographic model without BGS (π_0 - dashed colored lines) and with BGS (π - solid colored lines). (C) Relative diversity (π/π_0) measured by taking the ratio of diversity with BGS (π) to diversity without BGS (π_0) at each time point. Note that the x-axes in all three figures are on the same scale. Time is scaled using a human generation time of 25 years per generation. Simulation data was sampled every 100 generations.

S8 Fig. Simulations of diversity and relative diversity under BGS using various fractions of sites experiencing deleterious mutation. Values for the deleterious site

fraction are provided in the header for each set of plots. Left column plots show results of simulations under a demographic model with migration between all human populations. Right column plots show results of simulations under a demographic model with no migration. Colored lines represent different populations though time and are identical to those in Fig 5 and S7 Fig The demographic model used is also identical to that in Fig 5 (for simulations with migration) and S7 Fig (for simulations without migration). Simulation data was sampled every 100 generations.

S9 Fig. F_{ST} is not correlated with recombination rate.

F_{ST} measured across 2% recombination rate quantile bins. The right panel of S9 Fig displays a narrower range of recombination rates to show detail. Smaller transparent points and lines show the estimates and corresponding lines of best fit (using linear regression) for F_{ST} between every pairwise population comparison for a particular pair of continental groups (25 pairwise comparisons each). Larger opaque points and lines are mean F_{ST} estimates and lines of best fit across all Thousand Genomes Project (TGP) population comparisons between a particular pair of continental groups. Error bars represent ±1 SEM calculated from 1,000 bootstrapped datasets.

S10 Fig. F_{ST} between African (AFR) and South Asian (SASN) populations jointly across *B* and recombination rate.

(A) F_{ST} as a function of 25 recombination rate bins (4% quantile bins) conditional on three different 2% *B* quantile bins (note log scale of x-axis for recombination rate). (B) F_{ST} as a function of 25 *B* bins (4% quantile bins) conditional on three different 2% recombination rate quantile bins. Smaller transparent points and lines show the F_{ST} estimates and corresponding lines of best fit (using linear regression) for each of the pair-

wise comparisons of AFR vs. SASN Thousand Genomes Project (TGP) populations (25 comparisons total). Larger opaque points are mean F_{ST} estimates across all pairwise comparisons of AFR vs. SASN TGP populations (with bold lines showing their corresponding lines of best fit).

S11 Fig. Comparing patterns of diversity between local ancestry segments of admixed samples and continental groups.

(A) Normalized diversity (heterozygosity/divergence) and (B) Relative diversity: the ratio of normalized diversity in the lowest *B* quantile bins (strong BGS) in (A) to normalized diversity in the highest 1% *B* quantile bin (weak BGS). Local ancestry segments include African, European, and Native American ancestries. Continental groups include African, European, and East Asian populations. Error bars represent ±1 SEM calculated from 1,000 bootstrapped datasets.

S12 Fig. Simulations of singleton density and relative singleton density

A) Results of simulations under a demographic model with migration between all human populations. B) Results of simulations under a demographic model with no migration. The second row of A) and B) shows measurements of singleton density (i.e., number of singletons observed per site) from simulations without BGS (ψ_0 - dashed colored lines) and with BGS (ψ - solid colored lines). The bottom row of A) and B) shows corresponding relative singleton density (ψ/ψ_0) measured by taking the ratio of singleton density with BGS (ψ) to singleton density without BGS (ψ_0) at each sampled generation time point. The simulation data used for these measurements is identical to that of Fig 5 (for simulations with migration) and S7 Fig (for simulations without migration).

1301

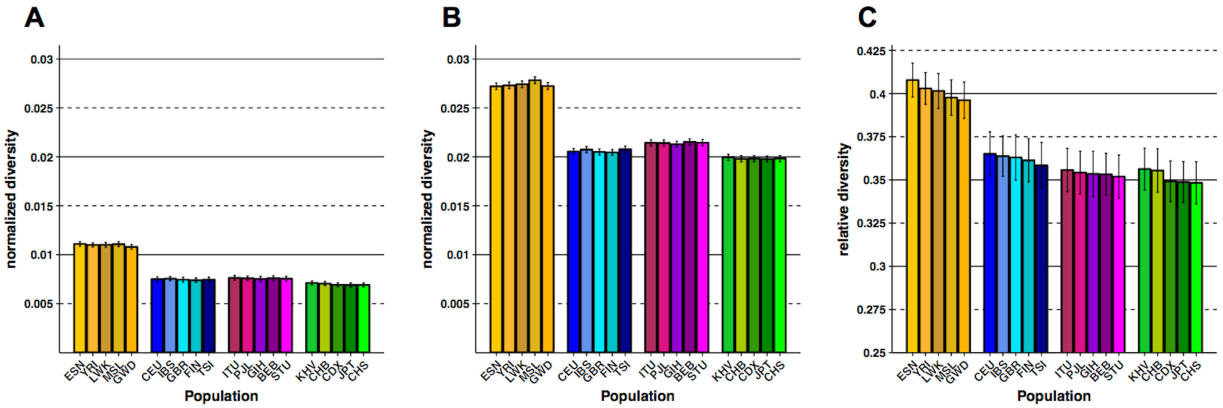

Fig 1. Normalized diversity and relative diversity for non-admixed populations of the Thousand Genomes Project (TGP).

(A) Normalized diversity (π/divergence) measured across the lowest 1% *B* quantile bin (strong BGS). (B) Normalized diversity measured across the highest 1% *B* quantile bin (weak BGS). (C) Relative diversity: the ratio of normalized diversity in the lowest 1% *B* bin to normalized diversity in the highest 1% *B* bin (π/π_0). TGP population labels are indicated below each bar (see S12 Table in Supporting information for population label descriptions), with African populations colored by gold shades, European populations colored by blue shades, South Asian populations colored by violet shades, and East Asian populations colored by green shades. Error bars represent ±1 SEM calculated from 1,000 bootstrapped datasets.

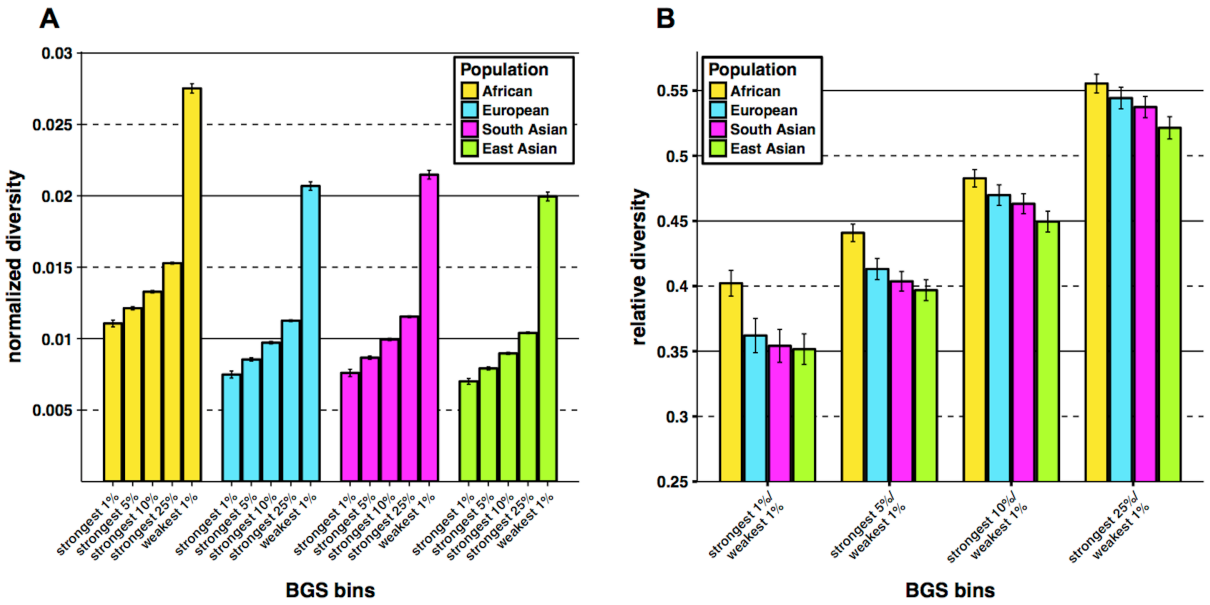

1315

1316 **Fig 2. Normalized and relative diversity for Thousand Genomes Project (TGP)**

1317 **continental groups**.

1318 (A) Normalized diversity (π/divergence) measured across the lowest 1%, 5%, 10% and

1319 25% *B* quantile bins (strong BGS) and the highest 1% *B* quantile bin (weak BGS). (B)

1320 Relative diversity: the ratio of normalized diversity in the lowest *B* quantile bins (strong

1321 BGS) in (A) to normalized diversity in the highest 1% *B* quantile bin (weak BGS). Error

1322 bars represent ±1 SEM calculated from 1,000 bootstrapped datasets.

1323

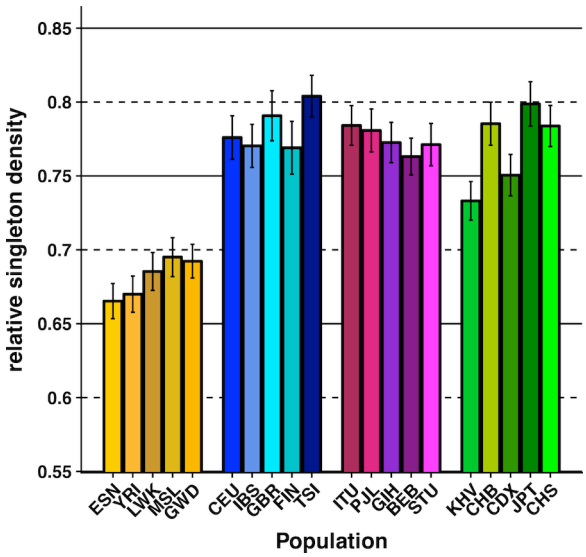

Fig 3. Relative singleton density for non-admixed populations of the Thousand Genomes Project (TGP).

Relative singleton density measured by taking the ratio of singleton density in the lowest 1% *B* quantile bin to singleton density in the highest 1% *B* quantile bin (ψ/ψ_0). Singleton density was normalized by divergence with Rhesus macaque. TGP population labels are indicated below each bar (see S12 Table in Supporting information for population label descriptions), with African populations colored by gold shades, European populations colored by blue shades, South Asian populations colored by violet shades, and East Asian populations colored by green shades. Error bars represent ±1 SEM calculated from 1,000 bootstrapped datasets.

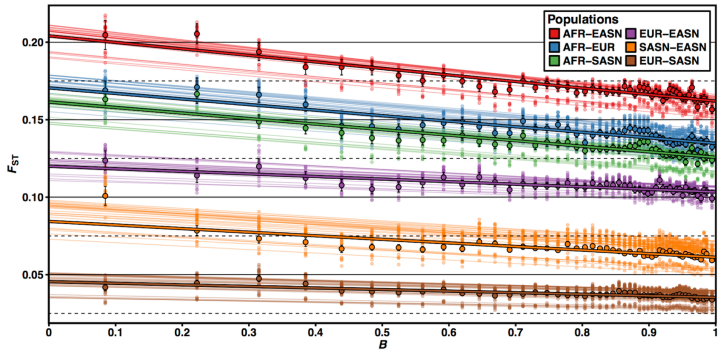

Fig 4. F_{ST} is correlated with *B*

F_{ST} measured across 2% quantile bins of *B*. Smaller transparent points and lines show the estimates and corresponding lines of best fit (using linear regression) for F_{ST} between every pairwise population comparison for a particular pair of continental groups (25 pairwise comparisons each). Larger opaque points and lines are mean F_{ST} estimates and lines of best fit across all Thousand Genomes Project (TGP) population comparisons between a particular pair of continental groups. Error bars represent ±1 SEM calculated from 1,000 bootstrapped datasets.

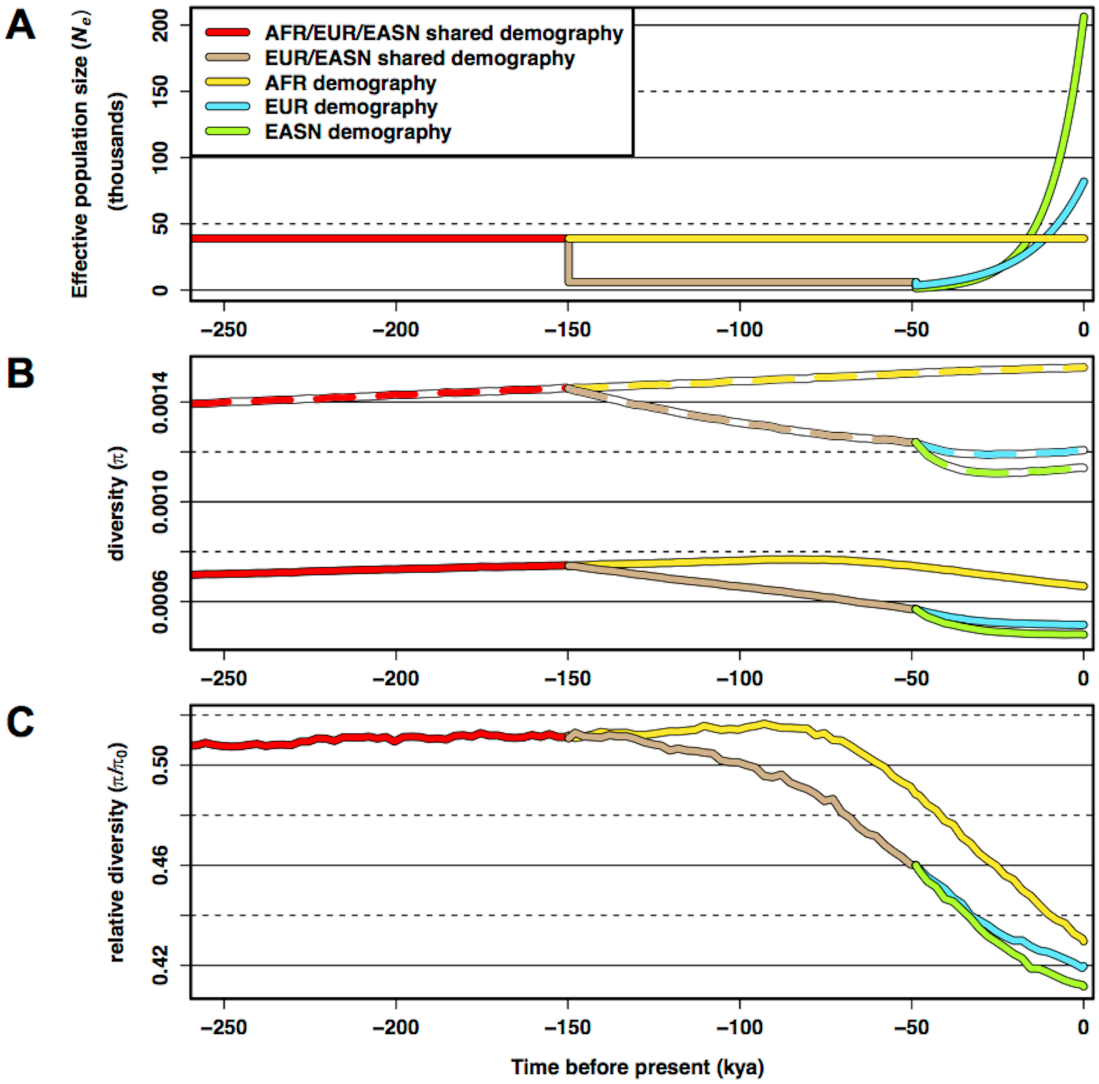

Fig 5. Simulations confirm that demographic events shape the impact of background selection (BGS).

(A) Inferred demographic model from Complete Genomics Thousand Genomes Project (TGP) data showing population size changes for Africans (AFR), Europeans (EUR), and East Asians (EASN) as a function of time that was used for the simulations of BGS. (B) Simulated diversity at neutral sites across populations as a function of time under our inferred demographic model without BGS (π_0 - dashed colored lines) and with BGS (π -

solid colored lines). (C) Relative diversity (π/π_0) measured by taking the ratio of diversity with BGS (π) to diversity without BGS (π_0) at each time point. Note that the x-axes in all three figures are on the same scale. Time is scaled using a human generation time of 25 years per generation. Simulation data was sampled every 100 generations.